Food Chemistry 480 (2025) 143865

Contents lists available at ScienceDirect

Food Chemistry

journal homepage: www.elsevier.com/locate/foodchem

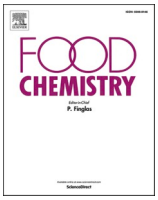

# Protein fractions in cow milk inhibit decontamination by cold atmospheric plasma

Ewa Tyczkowska-Sieroń [a], Ryszard Kapica [b], Ewelina Wielgus [c], Jacek Tyczkowski [b,*]

[a] Department of Experimental Physiology, Medical University of Lodz, Mazowiecka Str. 6/8, 92-215 Lodz, Poland
[b] Department of Molecular Engineering, Faculty of Process and Environmental Engineering, Lodz University of Technology, Wolczanska 213, 93-005 Lodz, Poland
[c] Centre of Molecular and Macromolecular Studies, PAS, Sienkiewicza 12, 90-363 Lodz, Poland

ARTICLE INFO

*Keywords:*
Cow milk
*Prototheca* algae
Cold plasma treatment
Hydroxyl radicals
Peptides

ABSTRACT

There is a growing body of research on the infection of cow milk by *Prototheca* algae, a potential human pathogen. This study presents investigations on plasma treatment to inactivate *Prototheca* directly in milk. However, microbiological tests revealed a surprisingly high survival rate of *Prototheca* in milk compared to saline solution treated under the same conditions. This phenomenon appears to be due to presence of proteins that act as scavengers of plasma reactive species, with $OH^{\bullet}$ radicals playing a major role. Studies using MALDI-TOF MS, FTIR, XPS and UV-VIS on a model solution of peptone K (simulating the molecular structure of milk protein fractions) confirmed the high reactivity of peptides with $OH^{\bullet}$ radicals, leading primarily to the substitution of hydrogen atoms with hydroxyl groups and cleavage of peptide chains. The obtained results encourage a broader consideration of proteins' role in plasma treatment processes, including applications in food products and plasma medicine.

## 1. Introduction

Cold plasma is emerging as an innovative and promising non-thermal technology for food decontamination. It has been tested across a wide range of applications, from meat and dairy products to fruits, juices, herbs, and spices (Hertwig et al., 2015; Murtaza et al., 2024; Pankaj et al., 2018; Surowsky et al., 2015). Despite extensive research on the effect of plasma on food products, including its impact on microorganisms and their killing, as well as on the modification of food ingredients, the mechanisms driving these processes are still not fully understood and are under active discussion (Gavahian et al., 2018; Liao et al., 2017; Sarangapani, Keogh, et al., 2017). This complexity arises from the variety of plasma types used (e.g., jet plasma, spark discharge, corona discharge, dielectric barrier discharge, low-pressure plasma), the wide range of its generation conditions, and the various procedures employed for plasma treatment (Kopuk et al., 2022; Moosavi et al., 2020; Zhou et al., 2020).

It is well-established that plasma's effects on food products are due to reactive species (free electrons, free radicals, ions, ion radicals, excited atoms and molecules) produced during its generation, typically using inert (non-polymerizing) working gases. Common gases in atmospheric-pressure plasma for food processing include argon, oxygen, nitrogen, or air. High-energy radicals like $O^{\bullet}$, $OH^{\bullet}$, $O_2^{\bullet-}$, $NO^{\bullet}$ are particularly reactive (Kopuk et al., 2022). However, these species have different lifetimes and concentrations, influenced by both generation conditions and the environment in which they act – this may be a gas phase (e.g., air) in the case of surface treatment of solid materials, or a liquid phase (aqueous solution) if liquids such as juices or milk are processed (Moszczyńska et al., 2023). Additionally, by-products resulting from the reactions of the plasma reactive species, such as $O_3$ (mainly in the gas phase) or $H_2O_2$ (primarily in the liquid phase), as well as UV radiation produced during plasma generation, should also be considered.

Setting aside the complex chemical structure of food components, the variety of plasma reactive species and the differences between gas and liquid phases in plasma reactions pose major challenges for developing even basic guidelines for specific plasma treatments. Each case currently requires a tailored approach based on dedicated research. This is especially true for aqueous solutions, where dissolved organic and inorganic substances can significantly influence plasma's biocidal activity (Hummert et al., 2023).

Milk, with its complex composition, exemplifies this challenge; its components significantly affect the plasma decontamination process (Nguyen et al., 2022). However, due to the thermal sensitivity of these components, cold plasma, as a non-thermal technology, appears to be a

* Corresponding author.
*E-mail address:* jacek.tyczkowski@p.lodz.pl (J. Tyczkowski).

https://doi.org/10.1016/j.foodchem.2025.143865
Received 17 November 2024; Received in revised form 9 March 2025; Accepted 10 March 2025
Available online 12 March 2025

promising solution (Coutinho et al., 2018; Rathod et al., 2021). Cold plasma treatment has attracted considerable interest as a method to ensuring microbiological safety in milk while preserving its sensory, nutritional, and physicochemical properties. At the same time, it is also seen as a tool for controlled modification of milk's structure and properties. Studies have examined various types of cow milk, including liquid forms such as raw, pasteurized, UHT, whole, semi-skimmed, and skimmed milk (Gurol et al., 2012; Kim et al., 2015; Korachi et al., 2015; Ponraj et al., 2017; Sharma & Singh, 2022) as well as powdered milk (Chen et al., 2019). Additionally, research has focused on freeze-dried bovine colostrum (Bogusławska-Wąs et al., 2023), isolated milk components in solid or liquid phases, such as sheep milk casein (Zhang et al., 2024), bovine milk casein and whey proteins (Ng et al., 2021; Segat et al., 2015), milk protein concentrate (Bormashenko et al., 2021), and the alkaline phosphatase enzyme naturally present in milk (Segat et al., 2016). Overall, despite challenges with plasma treatment technology, research supports its potential for milk decontamination and encourages further studies to expand its applications.

An important but underrecognized issue is the contamination of milk by *Prototheca* algae, a topic of increasing interest. Evidence suggests that milk and dairy products contaminated with *Prototheca*, such as butter and cheeses, may be sources of human infection (Abdelhameed, 2016; Libisch et al., 2022; Nardoni & Mancianti, 2023; Rivelli Zea et al., 2024). Removing this pathogen from milk is therefore as essential as eliminating other harmful microorganisms. However, *Prototheca* shows heat resistance and can survive high-temperature treatments (Lassa et al., 2011; Melville et al., 1999). Thus, alternative methods are needed to inactivate this pathogen in milk effectively.

A promising approach is the use of cold plasma. Our previous studies (Tyczkowska-Sieroń, Markiewicz, et al., 2018; Tyczkowska-Sieroń, Kapica, et al., 2018) demonstrated high sensitivity of *Prototheca zophii* to plasma treatment, with greater susceptibility than *Candida albicans* treated under similar conditions. However, these studies involved solid surface treatment (agar plates with pathogen cells spread uniformly for inhibition zone measurements). To date, no studies have been conducted on *Prototheca* inactivation directly in milk in the liquid phase.

Based on the results from solid surface studies, we hypothesized that plasma treatment could also effectively decontaminate liquid milk from *Prototheca*. Thus, the goal of this work was to verify plasma's efficacy in inactivating *Prototheca* cells in liquid milk without significantly altering its nutritional properties, and in the absence of positive results, to identify the underlying reasons.

## 2. Materials and methods

### 2.1. Materials

Commercial UHT cow milk (0.5 % fat) from Mlekpol Dairy Cooperative (Poland) was used for the tests. Skim milk samples were obtained by centrifuging it in a high-speed centrifuge (type 5430R, Eppendorf Poland Ltd.) at 12,700 rpm and 18,213 ×g for 30 min. Milk casein pancreatin hydrolysate, peptone K (hereinafter peptone), from BTL Ltd. (Poland) was used as a model protein substance in milk. The amino acid composition of peptone, its physicochemical characteristics, and molecular weight distribution, provided by the manufacturer, are listed in the Supplement in Tables S1, S2 and S3, respectively. Lactose monohydrate pure p.a. (Chempur, Poland) was used as a model substance for carbohydrates in milk. To study the activity of peptone in scavenging plasma reactive species, methylene blue trihydrate (MB) provided by Thermo Fisher GmbH (Germany, Catalog no.: J60823.30) was selected.

For microbiological tests, a sterile saline solution (API NaCl 0.85 % Medium; bioMérieux SA, France) was used (henceforth: saline). All other aqueous solutions were prepared using ultrapure water from a Millipore Direct–Q 3 UV system (Merck KGaA, Germany).

### 2.2. Plasma treatment system

Plasma treatment was performed using a cold atmospheric pressure plasma jet – kINPen 11 V (Neoplas GmbH, Germany) (Reuter et al., 2018). A schematic diagram of this plasma treatment system is provided by Fig. S1. The plasma jet model operates at a frequency of 1.0 MHz and a peak-to-peak voltage of 3.0 kV. Argon (99.999, Linde Gaz, Poland) was used as the feed gas with a flow rate of $10^3$ sccm. To control the plasma generation atmosphere, a shielding head device was used. Oxygen or nitrogen (both 99.999, Linde Gaz, Poland) at 100 sccm, controlled by SLA5850 flow meters (Brooks Instrument, USA), were used as shielding gas, along with versions of the same gases saturated with water vapor at room temperature. The plasma jet nozzle was positioned 8–10 mm from the surface of the treated solution. A Cimerec+ series magnetic stirrer, model SP88857108 (Thermo Scientific, USA), with a 6 mm diameter and 25 mm long glass-embedded dipole, stirred the solution at a speed of 120 rpm. Each time, a 4 mL solution was plasma treated in a 6.8 mm deep borosilicate glass Petri dish with a 47 mm internal diameter. Plasma treatment time ranged from 1 to 60 min depending on the solution. For direct plasma treatment of an agar substrate surface, the plasma jet nozzle was placed 15.2 mm above the surface, with a 3-min exposure time.

### 2.3. Microbiological tests

The reference strain of *Prototheca wickerhamii* (RE-4608014 ATCC 16529, American Type Culture Collection) was used in this study. An inoculum suspension of *P. wickerhamii* (hereinafter *Prototheca*) was prepared from a 72-h culture in saline, achieving an optical density of 0.5 on the McFarland scale (approx. $10^6$ CFU/mL), adjusted using a DEN-1B McFarland densitometer (SIA Biosan, Latvia). From this suspension, 50 µL was added to 5 mL of the test solution to obtain a test suspension with approx. $10^4$ CFU/mL. Test solutions included saline, 0.5 % fat milk, skimmed milk, and model solutions of peptone and lactose, with concentrations of 2.5 and 4.5 wt% respectively, reflecting typical milk protein and carbohydrate levels. A 50 µL sample of each test suspension, before and after plasma treatment, was inoculated onto Sabouraud dextrose agar (bioMérieux SA, France) Petri dishes and incubated at 35 °C for 72 h. Colony counts were recorded.

For direct plasma treatment of *Prototheca* cells pre-exposed to a solution, 100 µL of the cell suspension was spread evenly on Sabouraud dextrose agar, plasma-treated for 3 min, then incubated at 35 °C for 72 h, and inhibition zones were measured.

All plasma treatment experiments were repeated twice, with CFU counts performed in triplicate per experimental sample.

### 2.4. MALDI-TOF mass spectrometry

MALDI-TOF mass spectra were obtained using an Axima Performance instrument with a nitrogen laser (337 nm) (Shimadzu Corp., Japan). The pulsed extraction ion source accelerated ions to a kinetic energy of 20 keV. All data were collected in a positive-ion linear mode, with laser energy set just above threshold level. The system was externally calibrated using polyethylene glycol (PEG) standards (Merck KGaA, Germany). 2,5-dihydroxybenzoic acid (DHB, >99.0 % HPLC) (Merck KGaA, Germany) served as the matrix, prepared in 70/30 acetonitrile/water with 0.1 % trifluoroacetic acid (TFA, ≥99.0 %) (Merck KGaA, Germany) at 10 mg/mL. A 0.5 µL of peptone solution (untreated or plasma-treated) was mixed with 0.5 µL of matrix on the MALDI plate, dried, and then inserted into the mass spectrometer. Mass spectra were collected from a minimum 200 laser shots and processed using Biotech Launchpad ver. 2.9.1 (Shimadzu Corp., Japan).

### 2.5. FTIR spectrometry

FTIR spectra were recorded using a Jasco 6200 FTIR spectrometer

with a liquid nitrogen-cooled MCT detector (Jasco Inter. Co., Ltd., Japan). Aqueous peptone solutions (untreated or plasma-treated) were drop-coated onto ZnSe plates (Pike Technologies, USA) dried at 35 °C for 48 h, and vacuum-evaporated for an additional 24 h to remove all moisture. ZnSe plates with peptone samples were used for FTIR measurements in transmission mode. Spectra were collected from 5000 to 600 $cm^{-1}$ with 1 $cm^{-1}$ resolution, averaging 100 scans. Spectra were corrected by subtracting the substrate response.

### 2.6. XPS spectrometry

Elemental composition and chemical structure of peptone were analyzed by X-ray photoelectron spectroscopy (XPS) using a Kratos AXIS Ultra DLD spectrometer (Kratos Analytical Ltd., UK). Samples were deposited on a gold sheet as for ZnSe in FTIR. Monochromatic Al Kα X-rays (1486.6 eV) excited photoelectrons, with spectra collected from three 0.2 $mm^2$ spots per sample. Anode power was set to 180 W, and the electron analyzer pass energy to 20 eV for high-resolution measurements. Measurements used a charge neutralizer, and spectra were analyzed with Kratos Vision 2.2.10 software, calibrated to the Au $4f_{7/2}$ gold peak at 84.0 eV.

### 2.7. UV-VIS spectrometry

UV-VIS spectra were recorded using a UV-1800 spectrophotometer (Shimadzu Corporation, Japan) from 190 to 1100 nm with 1 nm steps. Quartz cuvettes (Thorlabs Inc., USA) of 10 mm and 1 mm path lengths were used. Peptone solutions, before and after plasma treatment, were tested in 1 mm cuvettes after 7-fold dilution in ultrapure water, used as the reference solution.

For methylene blue (MB) decolorization studies, 10 ppm MB solutions in ultrapure water and with added peptone were measured in 10 mm cuvettes, both without plasma treatment and after plasma treatment for 1 to 15 min. In all cases, analogous solutions without MB were used as references.

### 2.8. pH measurements

The pH measurements were performed using a CX-505 multifunctional laboratory instrument (Elmetron G.P., Poland) with a combined ERH-12-6 pH probe for small volumes. The probe was calibrated using standard buffers at pH 10.01, 7.01, and 4.01 (Hanna Instruments, Poland). For each test, 4.0 mL of solution was poured into a 10 mm vial, and the probe was immersed for the measurement.

### 2.9. Statistical analysis

Statistical analysis was conducted using Statistica software (version 6; StatSoft, Inc., USA). Results are presented as means ± their standard deviations. Differences between mean inactivation values were estimated with the difference test method, considering $p < 0.05$ as significant. Kinetics of MB decolorization and *Prototheca* inactivation were fitted by linear regression, with coefficient of determination ($r^2$) calculated.

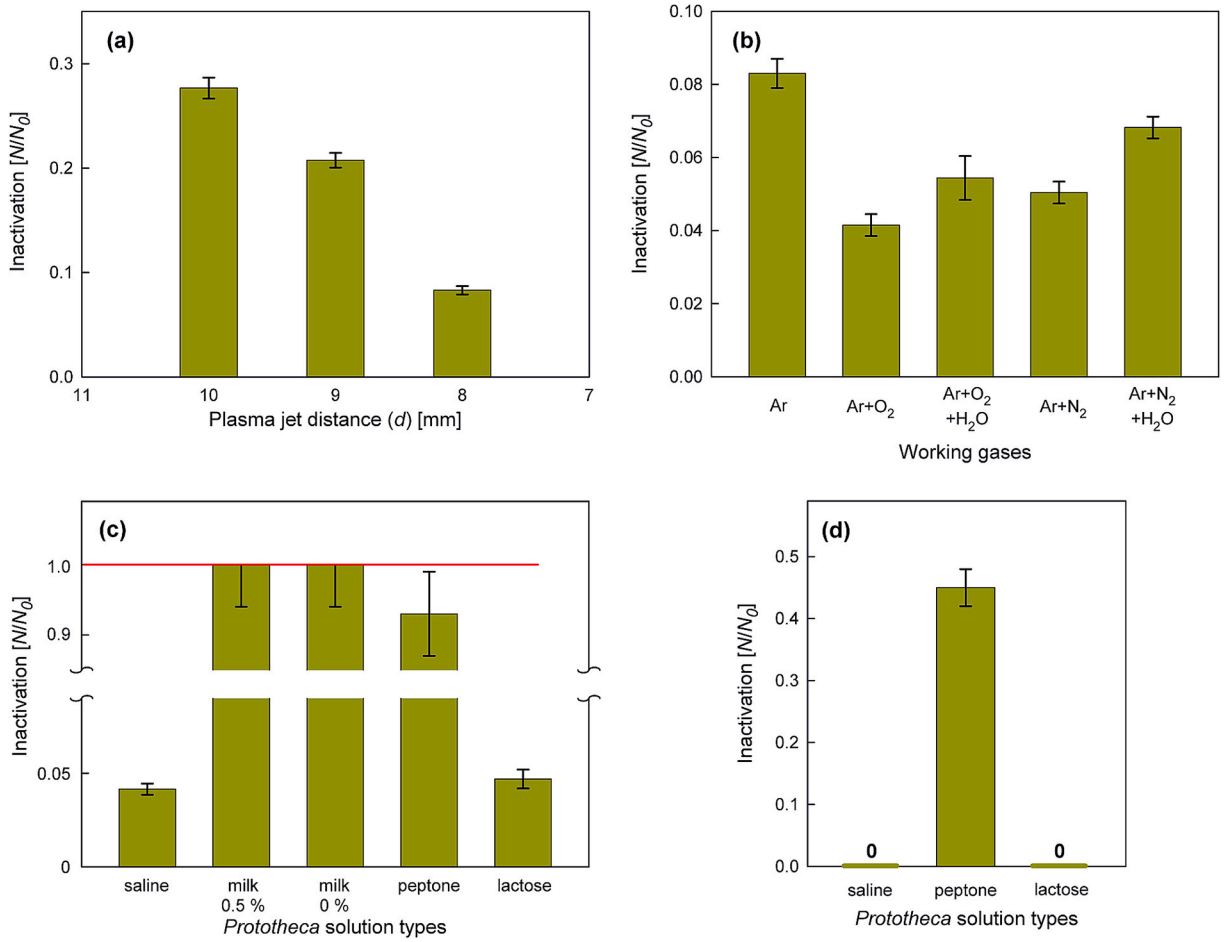


**Fig. 1.** Plasma-induced inactivation of *Prototheca* as a function of: (a) – plasma jet distance *d* (Ar plasma, 15 min treatment); (b) – working gas types ($d = 8$ mm, 15 min treatment); (c) – *Prototheca* solution types (Ar + $O_2$ plasma, $d = 8$ mm, 15 min treatment); (d) – *Prototheca* solution types (Ar + $O_2$ plasma, $d = 8$ mm, 60 min treatment). Examples of the raw data underlying the results presented in this figure are shown in the Supplementary data (Item 3).

## 3. Results

### 3.1. Microbiological analysis

The first stage of the study of *Prototheca* inactivation in milk was to determine the optimal parameters of plasma treatment, using a suspension of *Prototheca* cells ($10^4$ CFU/mL) in saline. Keeping the discharge power and gas flow rates fixed as described in Sec. 2.2, and assuming a plasma operation time of 15 min, we analyzed the influence of the jet distance (*d*) from the solution surface and the composition of the gas mixture in which the plasma was generated. Fig. 1(a) shows the dependence of *Prototheca* inactivation (expressed as the ratio of the number of surviving cells *N* to the initial number of cells $N_0$) as a function of the plasma jet distance during plasma generation in argon alone, while Fig. 1(b) shows the inactivation of *Prototheca* depending on the environment in which the plasma was generated, at a jet distance of 8 mm. Based on these results, all further studies on the effect of plasma on solutions, both with and without *Prototheca*, were carried out using plasma generated in Ar with an $O_2$ shielding gas ($Ar + O_2$) and an 8 mm jet distance, taking these conditions as standard.

A surprising result, confirmed several times, was the extremely weak effect of killing *Prototheca* cells in contaminated milk ($10^4$ CFU/mL) using the above-selected plasma treatment parameters. This contrasts with their suspension in saline subjected to the same treatment, where the process was much more intensive (Fig. 1(c)). This result indicates the important role of milk components, which likely involve very effective quenching of plasma reactive species, preventing them from contacting *Prototheca* cells and thereby blocking the possibility of their inactivation. To explain the causes of this phenomenon, it is necessary to determine which milk components are particularly responsible for the observed "quenching" of plasma and which plasma active species are primarily involved in this process.

The first component of milk whose effect on plasma deactivation was determined was fat. A sample of the same milk as before, only skimmed in the centrifugation process (Sec. 2.1), was taken for the study. This sample was then infected with *Prototheca* ($10^4$ CFU/mL) and treated with plasma. Unfortunately, no visible cell-killing effect was observed in this case either (Fig. 1(c)).

The next components of milk that were considered were proteins and carbohydrates. The studies were conducted in solutions simulating the presence of these milk components separately, thus allowing the determination of their individual effect on the survival of *Prototheca*. A model protein solution, an aqueous solution of peptone with a concentration of 2.5 wt%, was used, corresponding to the average casein content of milk. The model carbohydrate solution was prepared by dissolving lactose at a concentration of 4.5 wt% in water, which also corresponds to the average lactose content in milk. The results of the study on *Prototheca* inactivation in these solutions after exposure to plasma for 15 and 60 min are presented in Figs. 1(c) and 1(d). As shown, peptone significantly reduces the effect of plasma on *Prototheca* cells ($p < 0.05$), while lactose has no statistically significant effect ($p > 0.05$) compared to the saline solution. Therefore, it can be concluded that a special role in blocking the effect of plasma on *Prototheca* cells should be attributed to peptide structures.

Two possible scenarios of blocking the effect of plasma on *Prototheca* should be considered (Zhang et al., 2016). Firstly, we can assume that there is a permanent interaction between the *Prototheca* cell membrane and some of the peptide structures, which protects the cell surface and prevents access by plasma reactive species. Secondly, we can assume that the peptide structures are very active scavengers of plasma reactive species, rapidly reducing their concentration and thus the possibility of attacking *Prototheca* cells. To determine a probable scenario, tests of plasma treatment of *Prototheca* cultures inoculated on plates with a medium and measuring the inhibition zones were carried out. Culture samples were taken from *Prototheca*-infected solutions of pure saline, peptone, and lactose, mentioned above. An example of the test result is shown in Fig. 2. The lack of differences in the size of the inhibition zones clearly indicates the absence of permanent binding of the peptide structures with the cell membrane and protection of the cells from the action of plasma, which, in the case of such an effect, would be manifested by a reduction of the inhibition zone. Therefore, further research was directed toward exploring the second scenario and determining the role of peptide structures in the process of scavenging plasma reactive species.

### 3.2. Changes in the molecular composition of peptone by plasma treatment

The study of changes in the peptone structure regarding macromolecular composition caused by plasma action was performed using the MADI-TOF MS technique. Fig. 3(a) shows MALDI mass spectra for the raw peptone solution (the same as used in microbiological studies) and this solution subjected to plasma treatment for 15 and 60 min, collected for *m/z* 500–2500. Detailed results of the *m/z* range 500–1000, 1000–1200, 1200–1500, and 1600–2100 are shown in Figs. S3–S6. Due to the complex composition of the peptone mixture, accurately assigning peaks at a specific *m/z* values to the structure and sequence of amino acids in the peptide chains is very difficult based on the MALDI spectrum, but it is possible to attempt a general characterization of the changes occurring as a result of plasma treatment.

The first change that can be noticed in Fig. 3(a) is a decrease in the relative intensity of peaks in the higher *m/z* value region compared to the peaks at the lower *m/z* values. To confirm this tendency, the average molecular mass was estimated in the tested range of 500–2500 *m/z* as a comparative parameter using the simple equation:

$$\overline{M_I} = \frac{\sum_i \left[ I_i \bullet (m/z)_i \right]}{\sum_i I_i} \quad (1)$$

where $\overline{M_I}$ is the average molecular mass and $I_i$ is the peak intensity for a given $(m/z)_i$. The calculations assumed that under experimental conditions, almost exclusively singly charged ions are produced ($z = 1$) (Niessen & Falck, 2015). The obtained values are shown in Fig. 3(b). This result suggests that peptide molecules may be cleaved, leading to the formation of shorter chains by plasma treatment. Conversely, it can be assumed that free amino acids included in the peptone (Table S1), whose molecular mass is below 500 Da, undergo polycondensation as a result of the plasma action, forming short oligopeptide chains and thus enriching the content of components corresponding to lower *m/z* values in the studied range of 500–2000 *m/z*, which may also be manifested by a decrease in the average molecular mass in this range. However, studies conducted on the action of plasma on aqueous solutions of amino acids do not confirm this assumption (Takai et al., 2014; Zhou et al., 2016), leaving the cleavage of peptide chains as the more justified explanation (Kopuk et al., 2022; Liu et al., 2017).

The second effect of plasma action that can be concluded based on the results obtained from MALDI-TOF MS measurements is the change in the chemical structure of peptone as a result of interaction with reactive oxygen species leading to oxidation processes. In Fig. 3(a), in the MALDI mass spectrum of the peptone sample exposed to plasma for 15 min, additional peaks can be found at *m/z* values higher by 16 compared to the spectrum for the raw sample. For the peptone sample treated with plasma for 60 min, the peaks corresponding to the native peptide structures disappear significantly, and a clear increase in the peaks corresponding to the oxidized forms is observed. A telling example is the disappearance of the peak at *m/z* 1941.7 present in the mass spectrum of the raw peptone sample and the appearance of a distinct peak at *m/z* 1957.8 in the mass spectrum of the peptone sample treated with plasma for 60 min. A similar effect of an increase in molecular mass by 16 Da is also visible in the case of the peak at *m/z* 1854.5 transformed into the peak at *m/z* 1871.0, as well as the related peaks at *m/z* 1286.1 and

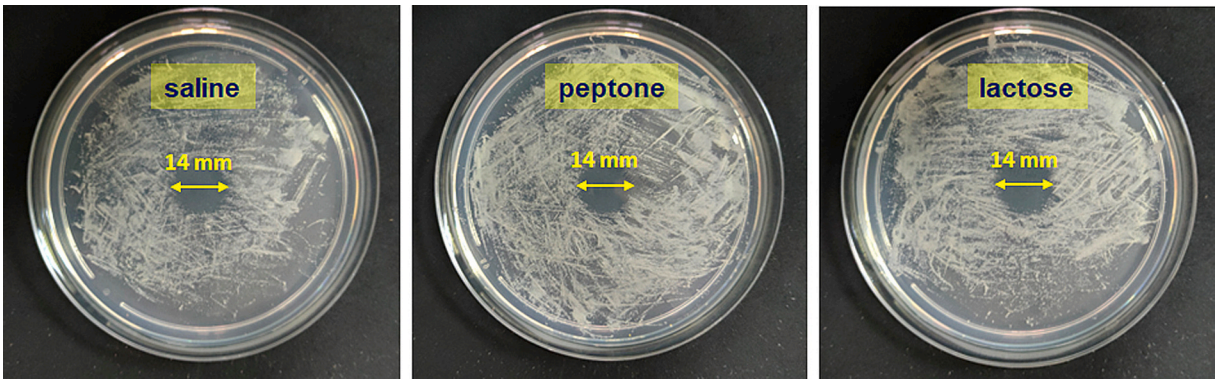


**Fig. 2.** *Prototheca* culture tests for suspension in saline, peptone and lactose solutions with distinct inhibition zones after jet plasma treatment (Ar + $O_2$ plasma, $d$ = 15.2 mm, 3 min treatment).

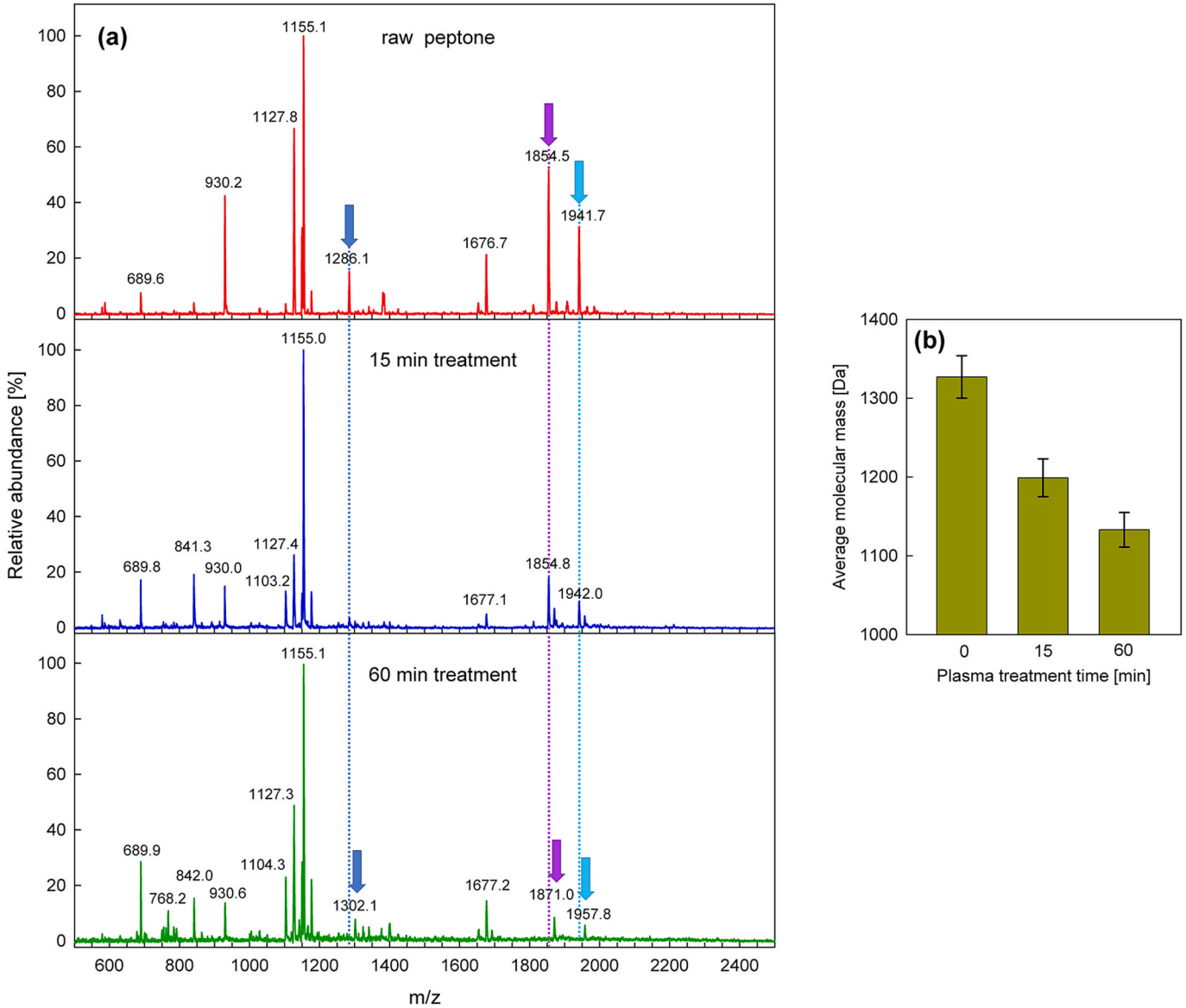


**Fig. 3.** MALDI-TOF MS results for peptone solution: (a) – mass spectra for untreated (raw) and plasma-treated for 15 and 60 min. The arrows indicate example peaks that shift by $m/z$ = +16, resulting from the binding of an oxygen atom to a given structure during plasma treatment.; (b) – estimated average molecular mass, according to eq. (1), as a function of plasma treatment time.

1302.4. These examples can be examined in more detail in Figs. S5 and S6.

The literature contains several reports indicating that amino acids in peptides are excellent targets for reactive oxygen species derived from plasma. A commonly observed modification is the introduction of one oxygen atom in the form of hydroxyl group (Verlackt et al., 2017; Wenske et al., 2021). Therefore, the change in the *m/z* values of peaks by 16 during plasma treatment can be interpreted in our case, for instance, as the replacement of the hydrogen atoms in C-H groups with hydroxyl groups. This will be confirmed by the FTIR and XPS results presented below.

### 3.3. Changes in the chemical structure of peptone by plasma treatment

To more precisely analyze the interaction of plasma reactive species with the components of peptone, changes in their chemical structure occurring during plasma treatment were examined. For this purpose, FTIR analysis, XPS spectrometry, and UV-VIS absorption spectrometry were employed.

#### 3.3.1. FTIR analysis

Fig. 4 shows FTIR spectra obtained in the range of 600–5000 $cm^{-1}$ for raw and plasma-treated (for 15 and 60 min) peptone samples. Although these spectra are very similar to each other, subtle differences can be found that should be attributed to the action of the plasma. These differences are primarily visible in the ranges 2850–3450, 1500–1700, and 800–950 $cm^{-1}$. The normalized FTIR spectra for these ranges are shown in Fig. S7(a), (b), and (c), respectively. As can be seen, with an increase in the plasma treatment time, there is a systematic increase in the intensity of the bands at 3273, 1646, 1588 and 845 $cm^{-1}$, along with a decrease in the intensity of the bands at 2962 $cm^{-1}$ and 922 $cm^{-1}$.

Due to the complex molecular structure of peptone, it is difficult to unambiguously assign specific bands to their corresponding functional groups. The literature reports several results regarding FTIR spectra for proteins (Barth, 2007; Poulsen et al., 2016; Seshadri et al., 1999; Szyk-Warszyńska et al., 2019; Whitehead et al., 2011) or specifically peptones (Trivedi, Branton, et al., 2015; Trivedi, Nayak, et al., 2015), as well as plasma-treated proteins (Jahromi et al., 2020; Ng et al., 2021; Zhang et al., 2024). Unfortunately, they are not unambiguous, and in interpreting our spectra, we must reference both the generally recognized data on infrared absorption spectra (Larkin, 2011; Silverstein et al., 2005; Stuart, 2004), and the MALDI-TOF MS studies presented above, as well as the XPS results discussed later.

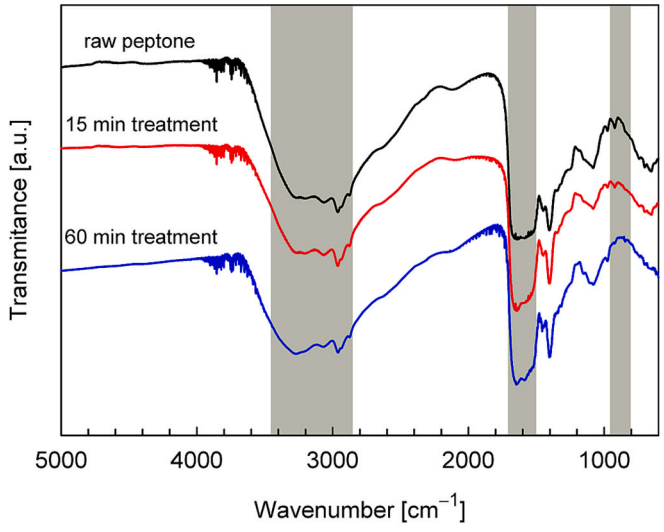


**Fig. 4.** FTIR spectra of untreated (raw) and plasma-treated (for 15 and 60 min) peptone samples. Spectrum ranges discussed in detail are marked in gray.

Regarding the band at 3273 $cm^{-1}$ (Fig. S7(a)), there is no doubt that the increase in its intensity during plasma exposure is attributable to an increase in the content of hydroxyl groups in the structure of the molecules that comprise peptone. The large width of this band suggests an increase in the number of intermolecular hydrogen bonds formed with the participation of the resulting −OH groups. In turn, the decrease in the intensity of the band at 2962 $cm^{-1}$, visible in the same figure, which arises from C−H stretching in alkanes, indicates partial abstraction of protons from carbon atoms of C−H bonds (Moosavi et al., 2020). It is likely that the hydrogen atoms are substituted with −OH groups, as suggested in Sec. 3.2.

Particularly important for the analysis of peptide structure is the IR absorption in the range of 1500–1700 $cm^{-1}$ (Fig. S7(b)). This range is usually assigned to the peptide bond (secondary amide), in which the amide I band (C=O stretch, near 1650 $cm^{-1}$) and amide II band (N−H bend and C−N stretch, near 1550 $cm^{-1}$) are distinguished. In practice, the amide I band is primarily used to assign secondary structures to proteins. Deconvolution of this band into individual sub-bands allows for the determination of the relative amounts of different secondary structures of proteins (α-helixes, β-sheets, turns, random coils) (Carbonaro & Nucara, 2010; Stuart, 2004). However, it should not be forgotten that there are also strong bands in this range associated with primary amines (N−H bend) and primary amides (C=O stretch), which can be correlated with the maxima visible in Fig. S7(b) at 1588 $cm^{-1}$ and 1646 $cm^{-1}$, respectively (Silverstein et al., 2005). The molecular mass distribution of the investigated peptone (Table S3), and the MALDI-TOF MS measurements (Fig. 3(a)), show that the peptide chains are mainly composed of several amino acid residues, reaching a maximum the length of about 10 amino acids. This practically excludes the possibility of observing a stable secondary structure of such chains (Ramirez-Alvarado et al., 1999; Su et al., 1994). The increase in band intensity in the range of 1500–1700 $cm^{-1}$ (Fig. S7(b)) should therefore be attributed to an increase in primary amine and primary amide groups due to the action of plasma on the peptone solution. This is consistent with expected changes in the chemical structure of peptone (e.g., resulting from chain cleavage) caused by reactive oxygen species, as supported by studies reported in the literature (Davies, 2005; Liu et al., 2017; Xu & Chance, 2007). However, it cannot be excluded that plasma-induced changes may occur in the secondary structure of the original milk proteins.

Some subtle but nevertheless clear changes were also observed in the 845 $cm^{-1}$ and 922 $cm^{-1}$ bands (Fig. S7(c)). The first of these bands, the intensity of which increases with the time of plasma exposure, can also be attributed, considering the XPS studies discussed later, to the wagging vibrations of N−H bonds in secondary amines (C−NH−C), which are one of the possible chemical moieties formed as a result of plasma-initiated transformations. The 922 $cm^{-1}$ band can be attributed to the P−O−P group and its out-of-phase stretching vibrations (Larkin, 2011), or, what seems more justified, to the P−O stretching vibrations in phosphate ions ($PO_4^{3-}$) (Nakamoto, 2009; Silverstein et al., 2005). The decrease in the intensity of this band during plasma exposure may be associated with the participation of P−O−P or $PO_4^{3-}$ groups, probably contained in some additional non-protein components of peptone derived from milk, in the formation of phosphate groups (e.g. C−O−$PO_3^{2-}$, C−N−$PO_3^{2-}$) located in the side chains of amino acids in the predicted phosphorylation process, the occurrence of which has already been proposed as a result of plasma treatment of sheep milk casein (Zhang et al., 2024). This interpretation requires further studies on the possible phosphorylation process occurring as a result of plasma exposure, but it is consistent with the XPS results presented below.

#### 3.3.2. XPS analysis

Deeper insights into the chemical structure of the studied peptone were obtained through XPS investigations. Fig. 5(a) shows typical low-resolution XPS wide scan spectra for peptone samples before and after plasma treatment. The presented spectra indicate that the tested samples

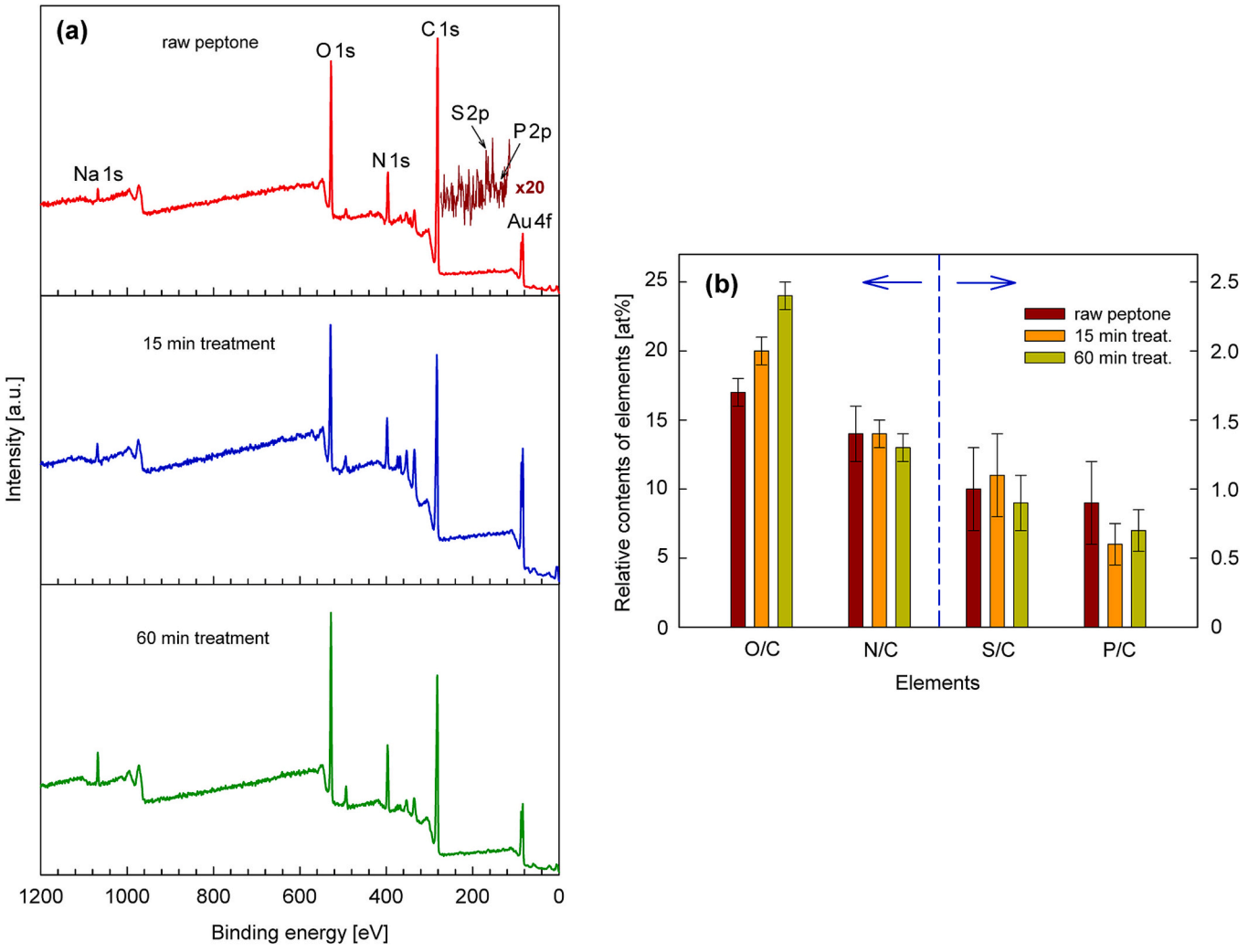


**Fig. 5.** XPS results for peptone samples: (a) – wide scans for untreated (raw) and plasma-treated for 15 and 60 min; (b) – relative contents of elements.

contain carbon, oxygen, nitrogen and a very small amount of sulfur – elements that are part of amino acids – as well as a minor quantity of phosphorus, whose origin and role were previously mentioned in the FTIR analysis. The spectra also identified the presence of sodium from NaCl, which is present at about 1 % in the tested peptone (Table S2), along with gold used as a substrate for the samples and as a reference material for calibration of the spectra.

At first glance, it is evident (by comparing the heights of the O 1s and C 1s bands) that the oxygen content increases relative to the carbon content with the duration of plasma treatment. Fig. 5(b) shows the relative contents of elements compared to the carbon content, which was assumed to be constant, as a function of the plasma treatment time. As observed, the oxygen content increases statistically significantly ($p < 0.05$) due to plasma action, as already pointed out in the MALDI-TOF MS (Sec. 3.2) and FTIR (Sec. 3.3.1) studies, and which should be associated with the action of reactive oxygen species on the components of peptone. The lack of significant changes in nitrogen content ($p > 0.05$) indicates the absence of reactive nitrogen species, which, despite the conditions of plasma generation in oxygen (Sec. 3.1), could appear as a result of further contact with air. No changes in the sulfur and phosphorus content are observed during plasma treatment either ($p > 0.05$), which seems justified.

However, the lack of changes in the elemental composition of peptone (except for oxygen) does not mean that the remaining molecular structure does not change apart from the emergence of new oxygen groups. To explore this issue, the core-level spectra of C 1s, N 1s, O 1s, S 2p, and P 2p were measured and subsequently numerically deconvoluted for further analysis. As with FTIR analysis, the mixture of many components in peptone and the high complexity of their chemical structure pose significant challenges in unequivocally determining the content of specific moieties and their changes during plasma treatment. Nevertheless, an attempt was made to identify the fundamental qualitative changes in the molecular structure of peptone observed as a result of plasma treatment, based on a wide range of XPS results reported in the literature (Table 1) and by correlating the conducted XPS analysis with our FTIR and MALDI-TOF MS results.

Fig. S8 shows examples of deconvoluted core-level spectra for the extreme cases studied: raw and 60 min plasma-treated peptone. Table 1 lists the binding energies (B.E.) for the fitted components shown in Fig. S8, their assigned chemical structures, atomic concentration (at.%), and references on which the band analysis was based.

The spectrum of carbon C 1s has been deconvoluted into five bands, whose relative intensity – and therefore the relative atomic concentration of the assigned groups – clearly changes as a result of plasma treatment. The $C_1$ band, due to the very low content of C=C bonds in the tested peptone (which can only be found in four amino acids: Phe, His, Trp, and Tyr (Table S1)), was assigned as a single band promarily to C – C and C – H connections (with a very small share of C=C). As a result of plasma treatment, the concentration of these bonds clearly decreases, while the concentration of C – OH bonds increases at a similar level ($C_3$

**Table 1**
XPS results for untreated (raw) and 60 min plasma-treated peptone samples. The table presents binding energies (B.E.) for the deconvoluted bands shown in Fig. S7, along with the assigned chemical structures, atomic concentrations (at.%), and relevant references used for band analysis.

| XPS spectrum | Band | Raw | | Plasma treatment 60 min | | Assignment | Ref. |
|---|---|---|---|---|---|---|---|
| | | B.E. | at. % | B.E. | at. % | | |
| C 1s | $C_1$ | 284.6 | 40.7 | 284.6 | 22.4 | C−H, C−C, C=C | (Artemenko et al., 2021; Ederer et al., 2017; Fears et al., 2013; Ganguly et al., 2011; Le Saux et al., 2016) |
| | $C_2$ | 285.6 | 19.7 | 285.3 | 23.6 | C**−N | |
| | $C_3$ | 286.2 | 13.7 | 286.2 | 29.8 | C−OH | |
| | $C_4$ | 287.7 | 21.7 | 287.9 | 19.1 | HN−C=O >C=O | |
| | $C_5$ | 289.0 | 4.2 | 289.0 | 5.1 | HO − C=O | |
| O 1s | $O_1$ | 530.8 | 46.3 | 530.8 | 33.1 | HN − C=O | (Artemenko et al., 2021; Ederer et al., 2017; Ganguly et al., 2011; He et al., 2022) |
| | $O_2$ | 531.5 | 35.8 | 531.4 | 40.0 | HO − C=O** > C=O | |
| | $O_3$ | 532.6 | 17.9 | 532.4 | 23.5 | HO** − C=O, C − OH | |
| | $O_4$ | – | – | 533.3 | 3.4 | N − O | |
| N 1s | $N_1$ | 399.6 | 80.9 | 399.6 | 49.5 | HN − C=O | (Abe & Watanabe, 2004; Artemenko et al., 2021; Ederer et al., 2017; Fears et al., 2013; Rao et al., 2014; Silva et al., 2012) |
| | $N_2$ | – | – | 400.2 | 14.9 | $H_2N$ − C=O | |
| | $N_3$ | 400.9 | 16.3 | 400.9 | 29.7 | C − $NH_2$ (C − $NH_3^+$) | |
| | $N_4$ | 402.0 | 2.8 | 402.1 | 5.9 | C − NH − C | |
| S 2p | $S_1$ | 164.1 | 46.7 | 164.0 | 10.3 | C − SH | (Adams et al., 2009; Siow et al., 2018; Varodi et al., 2021) |
| | $S_2$ | 165.1 | 53.3 | 165.1 | 11.0 | C − S − C | |
| | $S_3$ | – | – | 166.4 | 22.2 | C − SOH, C−(S=O) − C | |
| | $S_4$ | – | – | 168.3 | 39.9 | C − $SO_2H$, C−(O=S=O) − C | |
| | $S_5$ | – | – | 169.5 | 16.6 | C − $SO_3H$ | |
| P 2p | $P_1$ | 132.2 | 100 | – | – | P − O − P $PO_4^{3-}$ | (Amaral et al., 2005; Dake et al., 1989; Swift, 1982; Szczerska et al., 2023; Yao et al., 2022) |
| | $P_2$ | – | – | 133.5 | 100 | C − O − $PO_3^{2-}$ C − N − $PO_3^{2-}$ | |

(**) denotes the atom to which the band refers. It concerns moieties in which two atoms of the same element occur in different configurations. The standard deviation of atomic concentrations (at.%) is within ±5 %.

band). This confirms the process of hydrogen substitution with the −OH group in the C − H bond suggested by MALDI-TOF MS (Sec. 3.2) and FTIR (Sec. 3.3.1) studies due to the action of, for example, $OH^{\bullet}$ radicals (Wenske et al., 2021):

$$\sim C - H + OH^{\bullet} \rightarrow \sim C^{\bullet} + H_2O \quad (2)$$

$$\sim C^{\bullet} + OH^{\bullet} \rightarrow \sim C - OH \quad (3)$$

The $C_2$ band is assigned to carbon atoms (C**) in the C** − N bond, which can occur, for example, in a configuration such as a secondary amide (peptide bond) (∼C(=O) − NH − C**∼), a primary amine (∼C** − $NH_2$), or a secondary amine (∼C** − NH − C**∼). The small increase in C − N concentration observed as a result of plasma exposure (Table 1) can be interpreted as a result of the increase in the concentration of secondary amines and the decrease in C − N concentration due to the cleavage of this bond in the peptide bond and the formation of a primary amide (∼C(=O) − $NH_2$) (Davies, 2005). Secondary amines, present in small amounts in raw peptone (e.g. in amino acids Pro or Arg (Table S1)), may increase in concentration due to plasma action, for example according to the reaction (4) proposed below between ∼$C^{\bullet}$ radicals formed in reaction (2) and nitrogen-centered radicals formed in reaction (5) of peptide bond cleavage:

$$\sim C^{\bullet} + {}^{\bullet}NH - C^{**} \sim \rightarrow \sim C^{**} - NH - C^{**} \sim \quad (4)$$

$$\sim C(=O) - NH - C^{**} \sim + OH^{\bullet} \rightarrow \sim C(=O) - OH + {}^{\bullet}NH - C^{**} \sim \quad (5)$$

The $C_4$ and $C_5$ bands have been associated with the carbonyl group C=O bond occurring in the peptide bond and carboxyl group, respectively. The $C_4$ band can also be associated with carbonyl groups in the form of a ketone or aldehyde group (>C=O), which, although not expected in raw peptone, may appear as a result of plasma treatment. Plasma treatment generally causes a decrease in the intensity of the $C_4$ band and an increase in the intensity of the $C_5$ band. This can be explained by a decrease in the concentration of peptide bonds and an increase in the concentration of carboxyl groups (Table 1). This occurs, for example, as a result of reaction (5), which is associated with the cleavage peptide chains observed in MALDI-TOF MS studies. It should be added, however, that the cleavage of peptide chains at the NH−C** bond, leading to the formation of primary amide groups, does not change the intensity of the $C_4$ band. In contrast, the possible appearance of >C=O groups may increase its intensity.

The analysis of the oxygen O 1s spectrum (Table 1) regarding the C=O bond confirms a decrease in the concentration of peptide bonds (HN−C=O) ($O_1$ band) and an increase in the concentration of carboxyl groups (HO−C=O**) and ketone or aldehyde groups (>C=O) ($O_2$ band). The analysis concerning the C−O bond clearly confirms the increase in the concentration of hydroxyl groups (band $O_3$), which are primarily the result of reaction (3) but also of reaction (5). In addition to the aforementioned groups, another type of bond appears after plasma action, namely N−O, which has not been identified in raw peptone (band $O_4$). This bond likely forms due to nitrogen-centered radicals (e.g., as per reaction (5)) or according to the reaction (Hayon et al., 1970):

$$\sim C(=O) - NH - C \sim + OH^{\bullet} \rightarrow \sim C(=O) - N^{\bullet} - C \sim + H_2O \quad (6)$$

and subsequently participates in reactions involving oxygen ($O_2$) present in the plasma-treated solution or directly recombines with oxygen-centered radicals created during the action of plasma (Davies, 2005; Wenske et al., 2021).

The spectrum of nitrogen N 1s, resolved into four bands (with the $N_4$ band occurring only in plasma-treated peptone), confirms the changes in the chemical structure of peptone predicted above due to plasma treatment. The $N_1$ band, assigned to nitrogen atoms in the peptide bond, indicates a clear decrease in its concentration under the influence of plasma. The final result of peptide bond cleavage (∼C(=O)−NH−C∼) may involve its breaking at the C(=O)−|−NH site (e.g. reaction (5)), leading to an increase in the concentration of primary and secondary amine groups (reaction (4)), the $N_3$ and $N_4$ bands, respectively, as well as breaking at the NH−|−C site, resulting in the appearance of a primary amide ($N_2$ band).

The content of both sulfur and phosphorus in the studied peptone is very low (Fig. 5), so they should not be assigned any major role in the

global transformation of the chemical structure caused by plasma action. Nevertheless, for the sake of completeness, it is worth examining the changes occurring in the sulfur and phosphorus groups, which were detected despite very weak XPS signals.

The analyzed sulfur S 2p bands exhibited a doublet structure due to the presence of the S $2p_{3/2}$ and S $2p_{1/2}$ peaks. Therefore, they should be fitted using a 2:1 peak area ratio (S $2p_{3/2}$/S $2p_{1/2}$) and a 1.2 eV splitting (with lower binding energy for S $2p_{3/2}$) (Castner et al., 1996). Due to the low intensity of the S 2p spectra and the consequently higher noise level (Fig. S8), the separated S 2p bands assigned to specific groups were not subjected to further deconvolution and were treated as sums of the S $2p_{3/2}$ and S $2p_{1/2}$ peaks, similarly to what has been reported in other cases (Estevez et al., 2017). In raw peptone, two bands, $S_1$ and $S_2$, were identified, which were assigned to the C – SH and C – S – C groups (Table 1). These groups occur in very small amounts in peptone, being part of the chemical structure of cysteine and methionine, respectively (Table S1). Plasma treatment causes the oxidation of C – SH (Aranda-Rivera et al., 2022) and C – S – C (Davies, 2005) groups by reactive oxygen species, as revealed by the subsequent bands, $S_3$, $S_4$ and $S_5$, which were associated with sulfeno (C – SOH) and sulfinyl (C–(S=O) – C), sulfino (C – $SO_2H$) and sulfonyl (C–(O=S=O) – C), as well as sulfo (C – $SO_3H$) groups containing sulfur atoms in increasingly higher oxidation state, respectively.

The phosphorus P 2p bands, like the sulfur S 2p bands, consist of a doublet of P $2p_{3/2}$ and P $2p_{1/2}$, which peaks with an area ratio of 2:1 are split by a distance of 0.87 eV. Similarly to sulfur, the low intensity of the P 2p bands (Fig. S8) justifies the lack of their deconvolution into P $2p_{3/2}$ and P $2p_{1/2}$, leading to the analysis of the total P 2p bands, as is usually done (Amaral et al., 2005). In both raw and plasma-treated peptone, only a single P 2p band was found, which was clearly shifted toward higher binding energy as a result of the plasma treatment (Table 1). Based on the literature (Table 1), the P 2p band at 132.2 eV for raw peptone was assigned to the P – O – P or $PO_4^{3-}$ groups, while the P 2p band at 133.5 eV for peptone after plasma treatment was attributed to the phosphate moieties C – O – $PO_3^{2-}$ and C – N – $PO_3^{2-}$, thus confirming the results of the FTIR analysis (Sec. 3.3.1) and the possibility of the phosphorylation process under the influence of plasma (Zhang et al., 2024).

The C – O – $PO_3^{2-}$ and C – N – $PO_3^{2-}$ moieties are likely created as a result of reactions between the phosphate groups present in the peptone solution, originating from additional non-protein components, and carbon-centered and nitrogen-centered radicals formed in the side chains of amino acids by the action of hydroxyl radicals, according to the simple reactions: (Karpel Vel Leitner et al., 2002; Wenske et al., 2021):

$$\sim C - OH + OH^{\bullet} \rightarrow \sim C - O^{\bullet} + H_2O \quad (7)$$

$$\sim C - NH_2 + OH^{\bullet} \rightarrow \sim C - NH^{\bullet} + H_2O \quad (8)$$

### 3.3.3. UV-VIS absorption analysis

Fig. 6(a) shows absorption spectra in the range of 190–320 nm for an aqueous solution of raw (untreated) peptone and for this solution treated in plasma for 15 and 60 min. The spectra are presented as a dependence of the specific absorption coefficient (*A*) on the wavelength of light. Two bands with maxima at approximately 203 nm and 274 nm are clearly visible; then, as the wavelength of light increases, the absorption drops quickly, forming an absorption tail approaches zero and remains at this level throughout the entire visible light range. The revealed bands are typical for protein structures, where absorption in the range 180–230 nm is due almost entirely to $\pi \rightarrow \pi^*$ transitions in the peptide bonds, while the range 230–300 nm is associated with aromatic rings in amino acids such as Trp, Tyr, and Phe (Table S1) (Antosiewicz & Shugar, 2016; Nielsen & Schellman, 1967).

While the 203 nm band does not show any significant changes as a result of plasma treatment, the 274 nm band clearly changes its intensity (Fig. 6(b)). This indicates the elimination of aromatic rings as a result of the action of plasma reactive species. At this stage of research, it is difficult to clearly determine the path of this process and its products. For example, it may occur via an intermediate product, which is a hydroxycyclohexadienyl radical formed in the reaction of $OH^{\bullet}$ radicals with aromatic rings, as shown in the case of the amino acid Phe (Xu & Chance, 2007), leading to further reactions of this radical that remove aromatic conjugation. However, the most probable pathway appears to be the opening of the aromatic ring as a result of the action of $OH^{\bullet}$ radicals (Liang et al., 2021; Liang et al., 2024; Sarangapani, Danaher, et al., 2017). One of the products in this case are >C=O groups, which were mentioned in Sec. 3.3.2.

Another difference in the absorption spectrum between the raw peptone solution and the plasma-treated solution is visible in the absorption tails, where the *A* coefficient is noticeably higher as the plasma treatment time increases (Fig. 6(c)). It is assumed that in the case of protein solutions, absorption above 320 nm should be attributed exclusively to light scattering by the aggregates present (Padmanaban &

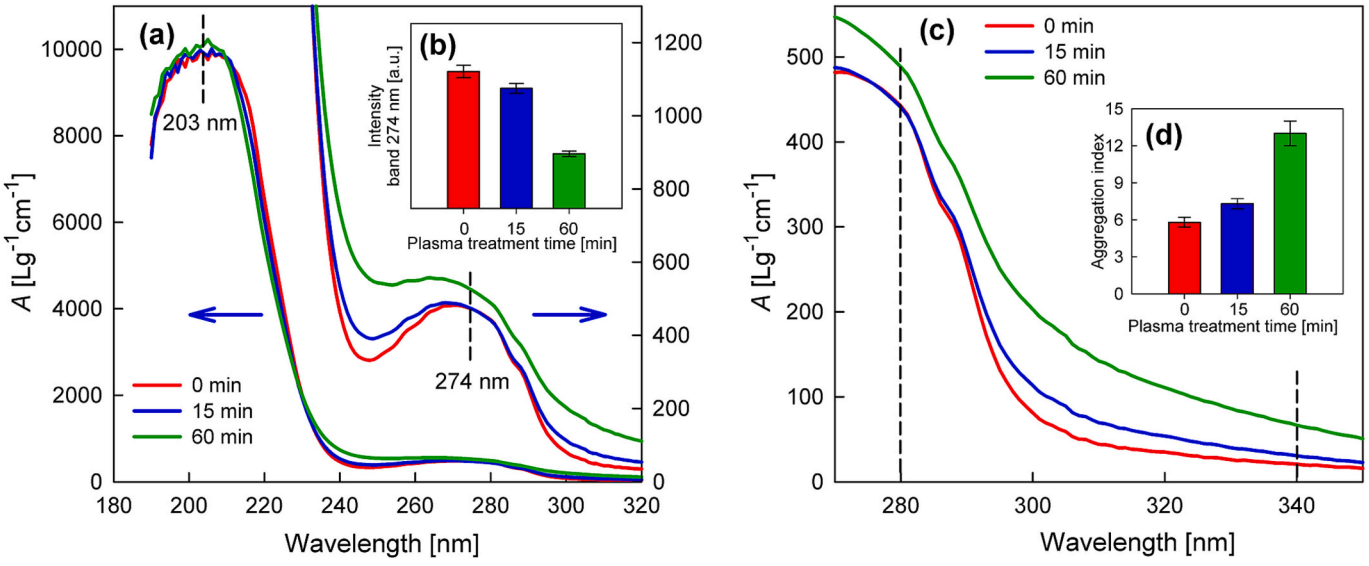


**Fig. 6.** UV-VIS results for untreated (0 min) and plasma-treaded for 15 and 60 min peptone solutions: (a) – absorption spectra in the 190–320 nm rage; (b) – 274 nm band intensity as a function of plasma treatment time; (c) – absorption tails in the 270–350 nm range; (*d*) – aggregation index (*AI*) as a function of plasma treatment time.

Menon, 2017; Raynal et al., 2014). As previously shown, during the action of plasma on the peptone solution, the concentration of hydroxyl groups increases in the peptide chains, which leads to increased aggregation through the formation of hydrogen bonds.

The parameter that describes the level of aggregation in a given system is the aggregation index (*AI*), determined according to the following equation (Katayama et al., 2005; Padmanaban & Menon, 2017):

$$AI = 100 \times \frac{A_{340}}{A_{280} - A_{340}} \quad (9)$$

where $A_{280}$ and $A_{340}$ denote the values of the specific absorption coefficient for 280 nm and 340 nm, respectively (Fig. 6(c)). Fig. 6(d) shows the aggregation index calculated in this way as a function of the plasma treatment time. After 60 min of plasma exposure, the *AI* value more than doubled, confirming the obvious increase in aggregation.

### 3.3.4. pH analysis

It is well known that the action of cold atmospheric plasma on water or aqueous solutions of various chemical compounds causes their acidification, sometimes even quite significantly. In the case of plasma generated in the air, the decrease in pH value is generally attributed to the formation of nitric and nitrous acids, although one should not overlook the products of chemical transformation of compounds present in solutions (Oehmigen et al., 2010; Sarangapani, Danaher, et al., 2017; Wang et al., 2022; Zhang et al., 2024; Zhou et al., 2016).

The pH measurements carried out on the aqueous solution of peptone tested by us before and after plasma treatment for 60 min showed only a slight decrease in pH value, from 6.90 ± 0.01 to 6.70 ± 0.03, respectively. The generation of plasma in oxygen (Sec. 3.1) and the XPS analysis (Sec. 3.3.2), which indicates a practical absence of chemical transformations resulting from the presence of reactive nitrogen species, justify the assumption that in this case, the formation of nitric acids can be neglected. The observed slight increase in acidity can be attributed to the establishment of acid-base balance under the new conditions, where the concentration of both acidic carboxyl groups and basic amino groups increases (Table 1).

## 3.4. Peptone activity in scavenging plasma reactive species

The plasma generated in oxygen, which was used in this work, is primarily a source of reactive oxygen species. XPS studies confirmed their intensive participation in the reconstruction of the chemical structure of peptone, indicating at the same time the lack of participation from potential reactive nitrogen species (Sec. 3.3.2). Among the oxygen species, hydroxyl radicals ($OH^{\bullet}$) play a particularly important role in plasma chemistry. They usually have a much higher concentration in the solution treated with plasma compared to other oxygen species, and also show much higher activity than the latter (Ji et al., 2019; Kanazawa et al., 2012). Therefore, $OH^{\bullet}$ should be considered a key factor in blocking the plasma interaction with *Prototheca* cells by proteins (Liu et al., 2017).

It has been found that a good quantitative indicator of $OH^{\bullet}$ is methylene blue (MB), which changes color from dark blue to colorless in the presence of these radicals in a sample solution (Satoh et al., 2007). The intensity of the band at approximately 664 nm in the UV-VIS absorption spectrum of the MB solution was used as a measure of MB concentration and applied to calculate its degradation as a function of plasma exposure time (Bansode et al., 2017; Tange et al., 2020). This relationship can be considered a reflection of $OH^{\bullet}$ concentration.

In the studies conducted in this work, an aqueous MB solution with a concentration of 10 ppm was used, in the form of a pure water solution and a solution with added peptone. Both the concentrations of peptone (2.5 wt%) and the plasma treatment procedure were the same as in the case of microbiological tests (Sec. 3.1). Fig. S9 shows the absorption spectra in the range of 500–750 nm for the tested solutions over different plasma treatment times. In each of these cases, a decrease in the intensity of the 664 nm band is visible with the duration of plasma exposure; however, the MB solution with peptone shows a much smaller change compared to the MB solution in pure water.

To quantitatively analyze these changes, pseudo-first-order kinetics was proposed to describe them (García et al., 2017):

$$ln\frac{A}{A_0} = kt \quad (10)$$

where $A_0$ and $A$ denote the absorbance of the 664 nm band for the initial solution and the solution after the time $t$ of plasma exposure, respectively, and $k$ is the apparent rate constant. Fig. 7 presents the results from Fig. S9 as the dependence of $\ln(A/A_0)$ as a function of $t$, which, as can be seen, fits eq. (10) with a high correlation ($r^2 > 0.99$). The determined values of the $k$ coefficient are also provided, which are in the range of those found for the plasma degradation of MB by other authors (Chandana et al., 2015; García et al., 2017). The obtained result clearly confirms the blocking effect of peptone, which scavenges $OH^{\bullet}$ radicals with high efficiency, reducing their concentration and, consequently, significantly reducing the degradation of MB.

## 4. Discussion

The studies conducted on the killing of *Prototheca* cells in cow milk using cold atmospheric plasma generated in a mixture of argon and oxygen clearly showed the practically absence of such an effect, whereas in an aqueous saline solution, very intense killing of these cells was observed (Fig. 1(c)). This result indicates the important role of milk components in quenching plasma reactive species and blocking their effect on *Prototheca* cells. To determine which milk components are particularly active in this blocking process, microbiological tests were carried out on skimmed milk and solutions of peptone and lactose. The concentrations of these solutions were similar to the concentrations of proteins and carbohydrates in average milk, amounting to 2.5 and 4.5 wt%, respectively. Based on the obtained results, it was determined that milk proteins are responsible for blocking the killing of *Prototheca* cells (Figs. 1(c) and 1(d)).

Further studies focused on determining the role of proteins in this process: how they they block the action of plasma reactive species on *Prototheca* cells, and what the mechanism of this process is. Direct

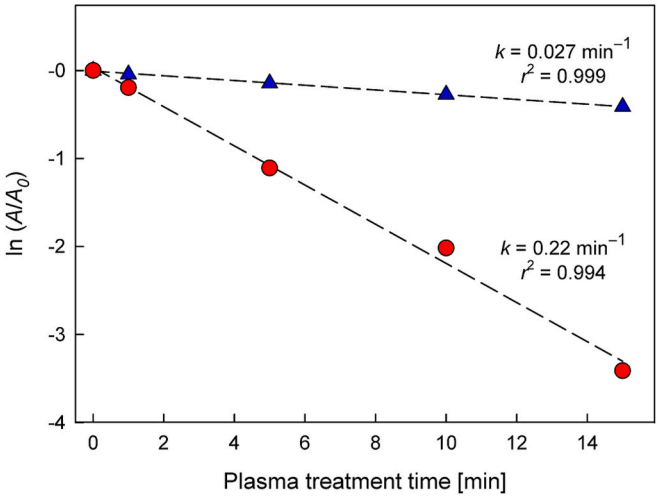


**Fig. 7.** Decolorization of methylene blue (MB) by plasma treatment, described by pseudo-first-order kinetics, according to eq. (10): ● – solution in water, ▲ – solution in water with added peptone ($k$ – apparent rate constant, $r^2$ – coefficient of determination). (For interpretation of the references to color in this figure legend, the reader is referred to the web version of this article.)

exposure of *Prototheca* cell cultures that had previously been in contact with peptone solution or saline solution showed no effect on their killing efficiency (Fig. 2). Thus, these results indicate a pathway for blocking the killing effect through intensive scavenging of plasma reactive species by components of peptone, preventing them from coming into contact with *Prototheca* cells. Taking into account the average size of the cells (about 6.5 μm in diameter) (Kano, 2020) and their initial number (about $10^4$ CFU/mL) (Sec. 2.3), it can be calculated that the ratio of their volume to the volume of the solution in which they are located is only $10^{-6}$. In contrast, the peptone solution, in terms of the number of its statistical molecules with an average molecular mass of 628 Da (Table S3), contains about $2.5 \times 10^{19}$ of them per mL. This justifies the conclusion that there is a significantly higher chance of contact between plasma reactive species and peptone molecules than with *Prototheca* cells.

As already mentioned, the plasma was generated in an oxygen-rich atmosphere, so mainly reactive oxygen species were expected. This was confirmed by XPS studies showing a clear increase in oxygen content in peptone and no change in nitrogen content after plasma treatment (Fig. 5(d)). Based on studies by other authors on the action of plasma on aqueous solutions (Ji et al., 2019; Kanazawa et al., 2012; Xu & Chance, 2007), it was assumed – which was confirmed by our results (MALDI-TOF MS, FTIR, XPS, UV-VIS) – that the reactive oxygen species with the highest concentration and reactivity in aqueous solution are hydroxyl radicals ($OH^{\bullet}$), which are responsible for the first step in the mechanism of plasma action on the peptone solution. These radicals in aqueous solution exist as $OH^{\bullet}(H_2O)_n$ hydrates, which can be present in solution for a long time and have similar chemical properties to isolated $OH^{\bullet}$ molecules (Zhou et al., 2016). Molecular dynamics simulations performed to provide atomic-scale insight into the initial interaction between $OH^{\bullet}$ and peptide systems in solution confirm the tremendous reactivity of these radicals, indicating that after only 10 ps nearly half of them have already reacted with the model peptide (Verlackt et al., 2017).

Blocking the killing of microbial cells by plasma reactive species in solutions containing additional dissolved substances has been reported several times, for example, in the presence of urea (Hummert et al., 2023) or bovine serum albumin (Zhang et al., 2016). A similar effect was also shown for the degradation of aflatoxins in milk using cold plasma, where the process occurred much more slowly than in standard solution (Nguyen et al., 2022). However, there is currently no deeper understanding of the reasons why the effective impact of plasma on a given substance or microorganism is blocked by another substance.

Some attempts to explain the behavior of proteins in this regard have attributed of this role to the sulfhydryl group (−SH) present in the amino acid cysteine (Cys) (Hummert et al., 2023; Zhang et al., 2016). This takes advantage of previous works on albumins, which pointed to the important role of the sulfhydryl group of Cys in quenching oxidative free radicals (Otagiri & Chuang, 2009; Di Simplicio, Cheeseman, & Slater, 1991). As a result of the reaction of the sulfhydryl group, for example, with the $OH^{\bullet}$ radical, it is oxidized to the sulfeno group −SOH, which is then further oxidized in the presence of reactive oxygen species to form the sulfino group $-SO_2H$ and finally the sulfo group $-SO_3H$ (Aranda-Rivera et al., 2022).

In our case, attributing the $OH^{\bullet}$ radical scavenging effect solely to the sulfhydryl groups in Cys (one −SH group per one Cys molecule) is unjustified considering the very low Cys content in peptone, which is 0.4 wt% (Table S1). This very low sulfur content was confirmed by XPS studies (Fig. 5(d)), which also showed an obvious effect of oxidation of −SH groups (Table 1, Fig. S8). However, this negligible effect, as already mentioned above, cannot explain the scavenging of reactive oxygen species.

The $OH^{\bullet}$ radical scavenging process should primarily be attributed to the substitution reactions of hydrogen atoms in the constituent peptone molecules (peptide chains and isolated amino acids (Table S1)) with hydroxyl groups (reactions (2) and (3)). The effective occurrence of these reactions as a result of plasma action was confirmed by FTIR (Fig. S7(a)) and XPS (Fig. S8, Table 1) studies. The increased concentration of −OH groups was also attributed to the aggregation effect, the occurrence of which was demonstrated based on UV-VIS optical absorption measurements (Figs. 6(c) and (d)).

Another important change in the chemical structure of peptone, which is a consequence of the initiating reaction with $OH^{\bullet}$ radicals, is the cleavage of peptide bonds (∼C(=O)−|−NH−||−C∼), manifested by the fragmentation of peptide chains, as demonstrated by MALDI-TOF MS studies (Fig. 3(a)). Such cleavage can take place at the (|) position, resulting in an increase in the concentration of carboxyl groups (reaction 5) and primary or secondary amine groups (reaction 4). In turn, cleavage at the (||) position leads to the appearance of primary amide groups. The above chemical changes occurring as a result of plasma action were indicated by FTIR studies (Figs. S7(b) and (c)) and XPS (Table 1).

Moreover, UV-VIS optical absorption studies revealed the process of opening aromatic rings (Figs. 6(a) and (b)). Such rings are present in the amino acids included in peptone: Phe (4.09 wt%), Trp (1.09 wt%), and Tyr (1.86 wt%) (Table S1). One of the likely products of aromatic ring opening may be carbonyl groups, presumably identified by XPS studies (Table 1).

Another process observed during the action of plasma on the peptone solution, which, due to its negligible intensity, does not play a significant role in the scavenging of $OH^{\bullet}$ radicals, is phosphorylation. Carbon-centered and nitrogen-centered radicals are formed in the side chains of amino acids by reaction with $OH^{\bullet}$ (reactions (7) and (8)), creating moieties such as $C-O-PO_3^{2-}$ and $C-N-PO_3^{2-}$. XPS studies indicate that such a process occurs (Table 1, Fig. S8).

The process of scavenging the main reactive oxygen species, $OH^{\bullet}$ radicals, by peptone, which has been adopted as a model for the molecular structure of protein fractions found in milk, drastically reduces the concentration of these radicals and the chance of contact with *Prototheca* cells, thus blocking the possibility of killing them. The very high efficiency of the $OH^{\bullet}$ reaction with peptone molecules was confirmed by the results of studies on the rate of decolorization of an aqueous solution of methylene blue (MB) under the action of plasma (Fig. 7). Assuming in the first approach that the determined values of the apparent rate constant $k$ can be represented as:

$$k = k^{'} C_{OH}^{\bullet} \tag{11}$$

where $C_{OH}^{\bullet}$ is a parameter proportional to the concentration of $OH^{\bullet}$ radicals decolorizing MB, the calculated decrease in this concentration after the addition of 2.5 wt% peptone is more than eightfold.

A simple estimation of the decrease in the concentration of $OH^{\bullet}$ responsible for the killing of *Prototheca* in the presence of peptone was also carried out, analogous to the above. Assuming, as in the case of decolorization of the MB solution, that the killing of *Prototheca* follows pseudo-first-order kinetics, modifying eq. (10) can be written:

$$ln\frac{N}{N_0} = kt \tag{12}$$

where $N_0$ is the initial number of cells, and $N$ is the number of cells that survived after time $t$ of plasma exposure. The relationship of $\ln(N/N_0)$ as a function of $t$, based on the results in Figs. 1(c) and (d), is shown in Fig. S10. Then using eq. (11), where $C_{OH}^{\bullet}$ is now a parameter proportional to the concentration of $OH^{\bullet}$ killing *Prototheca* cells, it can be calculate that the decrease in this concentration in the presence of peptone, which plays the role of $OH^{\bullet}$ scavenger, is fifteenfold, a similar order to that determined for MB decolorization.

From Fig. S10, it is also possible to estimate the plasma treatment time required to achieve the same inactivation of *Prototheca* as with a 15-min plasma treatment of a suspension with the same initial cell count in saline solution. This time is about 230 min, which disqualifies the use of cold plasma as a method for decontaminating liquid milk from *Prototheca*, if only because of the very significant changes in the chemical structure of proteins, the occurrence of which after such a long period of

plasma treatment is evident from the studies discussed above.

## 5. Conclusions

The primary conclusion of this work is the clear demonstration of the important role of protein fractions in blocking cold plasma-induced inactivation of microorganisms present in their surrounding environment. Detailed studies conducted on *Prototheca*-infected cow milk did not confirm the hypothesis posed in the Introduction (Sec. 1) – namely, that plasma treatment would be an effective method for decontaminating liquid milk from *Prototheca*. It was established that the main reason for this failure is precisely the presence of the protein in the milk.

Studies conducted on an aqueous suspension of *Prototheca* cells, with peptone used as a milk protein model system and cold plasma generated in an oxygen atmosphere, showed that the blocking effect on cells inactivation is due to the highly effective reactivity of peptone components with reactive oxygen species, among which the hydroxyl radicals $OH^{\bullet}$ plays a predominant role. The molecules of peptone components act as $OH^{\bullet}$ scavengers, rapidly reducing the radicals' concentration and thus their ability to react with cells. This increases cell survival rates many times over compared to studies performed on a suspension without protein structures.

It was determined that the mechanism of $OH^{\bullet}$ scavenging by peptone primarily involves the substitution of hydrogen atoms in peptide chains, as well as in isolated amino acids, with hydroxyl groups. Additionally, we observe the cleavage of peptide chains, leading to the formation of carboxyl, primary and secondary amine, and primary amide groups. To a lesser extent, reactions also include cleavage of aromatic rings, oxidation of sulfhydryl groups, and phosphorylation. All these reactions alter the chemical and physicochemical properties of peptides, which, given the prolonged plasma treatment time required to achieve sufficient *Prototheca* inactivation, disqualifies plasma treatment as a simple method of milk decontamination that does not alter the product properties.

The high reactivity of protein fractions with reactive oxygen species, mainly $OH^{\bullet}$ radicals, generated by cold oxygen plasma, demonstrated both directly in milk and in peptone solution, undoubtedly has a broader significance beyond this particular attempt to decontaminate cow milk. The reactions described above – driven solely by the molecular structure of the amino acids forming peptide chains – are of a general nature and can be expected to occur in any instance of plasma action on proteins.

Cold plasma is increasingly being tested in food processing, agriculture (for plasma-activated seed treatments), and plasma medicine. It is essential to consider that in all these applications, the presence of proteins in plasma-treated objects will undoubtedly influence the outcome of the process.

## CRediT authorship contribution statement

**Ewa Tyczkowska-Sieroń:** Writing – original draft, Methodology, Investigation, Formal analysis, Conceptualization. **Ryszard Kapica:** Methodology, Investigation, Formal analysis. **Ewelina Wielgus:** Methodology, Investigation, Formal analysis. **Jacek Tyczkowski:** Writing – review & editing, Writing – original draft, Visualization, Supervision, Methodology, Formal analysis, Conceptualization.

## Declaration of competing interest

The authors declare that they have no known competing financial interests or personal relationships that could have appeared to influence the work reported in this paper.

## Acknowledgements

This work was financially supported by the statutory funds of Lodz University of Technology (LUT). The authors express their sincere gratitude to Prof. Dorota Kręgiel of LUT for her valuable discussions and support throughout this research, and to Dr. Maciej Fronczak of LUT for his assistance with FTIR and XPS measurements.

## Appendix A. Supplementary data

Supplementary data to this article can be found online at https://doi.org/10.1016/j.foodchem.2025.143865.

## Data availability

Data will be made available on request.

## References

Abdelhameed, K. G. (2016). Detection of *Prototheca zopfii* in raw milk and cheese with special reference to their antibiogram. *Journal of Food Safety, 36*(2), 214–219. https://doi.org/10.1111/jfs.1223334

Abe, T., & Watanabe, A. (2004). X-ray photoelectron spectroscopy of nitrogen functional groups in soil humic acids. *Soil Science, 169*(1), 35–43. https://doi.org/10.1097/01.ss.0000112016.97541.28

Adams, L., Oki, A., Grady, T., McWhinney, H., & Luo, Z. (2009). Preparation and characterization of sulfonic acid-functionalized single-walled carbon nanotubes. *Physica E, 41*(4), 723–728. https://doi.org/10.1016/j.physe.2008.11.018

Amaral, I. F., Granja, P. L., & Barbosa, M. A. (2005). Chemical modification of chitosan by phosphorylation: An XPS, FT-IR and SEM study. *Journal of Biomaterials Science, Polymer Edition, 16*(12), 1575–1593. https://doi.org/10.1163/156856205774576736

Antosiewicz, J. M., & Shugar, D. (2016). UV–Vis spectroscopy of tyrosine side-groups in studies of protein structure. Part 2: Selected applications. *Biophysical Reviews, 8*(2), 163–177. https://doi.org/10.1007/s12551-016-0197-7

Aranda-Rivera, A. K., Cruz-Gregorio, A., Arancibia-Hernández, Y. L., Hernández-Cruz, E. Y., & Pedraza-Chaverri, J. (2022). RONS and oxidative stress: An overview of basic concepts. *Oxygen, 2*(4), 437–478. https://doi.org/10.3390/oxygen2040030

Artemenko, A., Shchukarev, A., Štenclová, P., Wagberg, T., Segervald, J., Jia, X., & Kromka, A. (2021). Reference XPS spectra of amino acids. *IOP Conference Series: Materials Science and Engineering, 1050*, article 012001. doi:https://doi.org/10.1088/1757-899X/1050/1/012001.

Bansode, A. S., More, S. E., Siddiqui, E. A., Satpute, S., Ahmad, A., Bhoraskar, S. V., & Mathe, V. L. (2017). Effective degradation of organic water pollutants by atmospheric non-thermal plasma torch and analysis of degradation process. *Chemosphere, 167*, 396–405. https://doi.org/10.1016/j.chemosphere.2016.09.089

Barth, A. (2007). Infrared spectroscopy of proteins. *Biochimica et Biophysica Acta, 1767*(9), 1073–1101. https://doi.org/10.1016/j.bbabio.2007.06.004

Bogusławska-Wąs, E., Dłubała, A., Sawicki, W., Ożgo, M., & Lepczyński, A. (2023). The effect of cold plasma on selected parameters of bovine colostrum. *Applied Sciences, 13*, Article 5490. https://doi.org/10.3390/app13095490

Bormashenko, E., Bormashenko, Y., Legchenkova, I., & Eren, N. M. (2021). Cold plasma hydrophilization of soy protein isolate and milk protein concentrate enables manufacturing of surfactant-free water suspensions. Part I: Hydrophilization of food powders using cold plasma. *Innovative Food Science and Emerging Technologies, 72*, Article 102759. https://doi.org/10.1016/j.ifset.2021.102759

Carbonaro, M., & Nucara, A. (2010). Secondary structure of food proteins by Fourier transform spectroscopy in the mid-infrared region. *Amino Acids, 38*(3), 679–690. https://doi.org/10.1007/s00726-009-0274-3

Castner, D. G., Hinds, K., & Grainger, D. W. (1996). X-ray photoelectron spectroscopy sulfur 2p study of organic thiol and disulfide binding interactions with gold surfaces. *Langmuir, 12*(21), 5083–5086. https://doi.org/10.1021/la960465w

Chandana, L., Reddy, M. K., & P., & Subrahmanyam, C.. (2015). Atmospheric pressure non-thermal plasma jet for the degradation of methylene blue in aqueous medium. *Chemical Engineering Journal, 282*, 116–122. https://doi.org/10.1016/j.cej.2015.02.027

Chen, D., Peng, P., Zhou, N., Cheng, Y., Min, M., Ma, Y., Mao, Q., Chen, P., Chen, C., & Ruan, R. (2019). Evaluation of *Cronobacter sakazakii* inactivation and physicochemical property changes of non-fat dry milk powder by cold atmospheric plasma. *Food Chemistry, 290*, 270–276. https://doi.org/10.1016/j.foodchem.2019.03.149

Coutinho, N. M., Silveira, M. R., Rocha, R. S., Moraes, J., Ferreira, M. V. S., Pimentel, T. C., … Cruz, A. G. (2018). Cold plasma processing of milk and dairy products. *Trends in Food Science & Technology, 74*, 56–68. https://doi.org/10.1016/j.tifs.2018.02.008

Dake, L. S., Baer, D. R., & Friedrich, D. M. (1989). Auger parameter measurements of phosphorus compounds for characterization of phosphazenes. *Journal of Vacuum Science & Technology A, 7*(3), 1634–1638. https://doi.org/10.1116/1.576062

Davies, M. J. (2005). The oxidative environment and protein damage. *Biochimica et Biophysica Acta, 1703*, 93–109. https://doi.org/10.1016/j.bbapap.2004.08.007

Di Simplicio, P., Cheeseman, K. H., & Slater, T. F. (1991). The reactivity of the SH group of bovine serum albumin with free radicals. *Free Radical Research Communications, 14*(4), 253–262. https://doi.org/10.3109/10715769109088954

Ederer, J., Janoš, P., Ecorchard, P., Tolasz, J., Štengl, V., Beneš, H., Perchacz, M., & Pop-Georgievski, O. (2017). Determination of amino groups on functionalized graphene

oxide for polyurethane nanomaterials: XPS quantitation vs. functional speciation. *RSC. Advances, 7*(21), 12464–12473. https://doi.org/10.1039/c6ra28745j
Estevez, R., Iglesias, I., Luna, D., & Bautista, F. M. (2017). Sulfonic acid functionalization of different zeolites and their use as catalysts in the microwave-assisted etherification of glycerol with tert-butyl alcohol. *Molecules, 22*, Article 2206. https://doi.org/10.3390/molecules22122206
Fears, K. P., Petrovykh, D. Y., & Clark, T. D. (2013). Evaluating protocols and analytical methods for peptide adsorption experiments. *Biointerphases, 8*, Article 20. https://doi.org/10.1186/1559-4106-8-20
Ganguly, A., Sharma, S., Papakonstantinou, P., & Hamilton, J. (2011). Probing the thermal deoxygenation of graphene oxide using high-resolution in situ X-ray-based spectroscopies. *Journal of Physical Chemistry C, 115*(34), 17009–17019. https://doi.org/10.1021/jp203741y
García, M. C., Mora, M., Esquivel, D., Foster, J. E., Rodero, A., Jiménez-Sanchidrián, C., & Romero-Salguero, F. J. (2017). Microwave atmospheric pressure plasma jets for wastewater treatment: Degradation of methylene blue as a model dye. *Chemosphere, 180*, 239–246. https://doi.org/10.1016/j.chemosphere.2017.03.126
Gavahian, M., Chu, Y. H., Khaneghah, A. M., Barba, F. J., & Misra, N. N. (2018). A critical analysis of the cold plasma induced lipid oxidation in foods. *Trends in Food Science & Technology, 77*, 32–41. https://doi.org/10.1016/j.tifs.2018.04.009
Gurol, C., Ekinci, F. Y., Aslan, N., & Korachi, M. (2012). Low temperature plasma for decontamination of *E. coli* in milk. *International Journal of Food Microbiology, 157*(1), 1–5. https://doi.org/10.1016/j.ijfoodmicro.2012.02.016
Hayon, E., Ibata, T., Lichtin, N. N., & Simic, M. (1970). Sites of attack of hydroxyl radicals on amides in aqueous solution. *Journal of the American Chemical Society, 92*(13), 3898–3903. https://doi.org/10.1021/ja00716a011
He, X., Liu, B., Zhang, S., Li, H., Liu, J., Sun, Z., & Chang, H. (2022). Nickel nitrate hydroxide holey nanosheets for efficient oxygen evolution electrocatalysis in alkaline condition. *Electrocatalysis, 13*(1), 37–46. https://doi.org/10.1007/s12678-021-00686-3
Hertwig, C., Reineke, K., Ehlbeck, J., Erdoğdu, B., Rauh, C., & Schlüter, O. (2015). Impact of remote plasma treatment on natural microbial load and quality parameters of selected herbs and spices. *Journal of Food Engineering, 167*, 12–17. https://doi.org/10.1016/j.jfoodeng.2014.12.017
Hummert, M., Leenders, P., Mellmann, A., Becker, K., & Kuczius, T. (2023). Generation of plasma-activated fluids for successful disinfection of *Pseudomonas aeruginosa* in liquid environments and determination of microbial damage. *Plasma, 6*(4), 699–713. https://doi.org/10.3390/plasma6040048
Jahromi, M., Niakousari, M., Golmakani, M. T., Ajallouеian, F., & Khalesi, M. (2020). Effect of dielectric barrier discharge atmospheric cold plasma treatment on structural, thermal and techno-functional characteristics of sodium caseinate. *Innovative Food Science and Emerging Technologies, 66*, Article 102542. https://doi.org/10.1016/j.ifset.2020.102542
Ji, W. O., Lee, M. H., Kim, G. H., & Kim, E. H. (2019). Quantitation of the ROS production in plasma and radiation treatments of biotargets. *Scientific Reports, 9*, Article 19837. https://doi.org/10.1038/s41598-019-56160-0
Kanazawa, S., Furuki, T., Nakaji, T., Akamine, S., & Ichiki, R. (2012). Measurement of OH radicals in aqueous solution produced by atmospheric-pressure LF plasma jet. *International Journal of Plasma Environmental Science & Technology, 6*(2), 166–171. https://doi.org/10.34343/ijpest.2012.06.02.166
Kano, R. (2020). Emergence of fungal-like organisms: *Prototheca*. *Mycopathologia, 185*, 747–754. https://doi.org/10.1007/s11046-019-00365-4
Karpel Vel Leitner, N., Berger, P., & Legube, B. (2002). Oxidation of amino groups by hydroxyl radicals in relation to the oxidation degree of the α-carbon. *Environmental Science and Technology, 36*(14), 3083–3089. https://doi.org/10.1021/es0101173
Katayama, D. S., Nayar, R., Chou, D. K., Campos, J., Cooper, J., Vander Velde, D. G., … Manning, M. C. (2005). Solution behavior of a novel type 1 interferon, interferon-τ. *Journal of Pharmaceutical Sciences, 94*(12), 2703–2715. https://doi.org/10.1002/jps.20461
Kim, H. J., Yong, H. I., Park, S., Kim, K., Choe, W., & Jo, C. (2015). Microbial safety and quality attributes of milk following treatment with atmospheric pressure encapsulated dielectric barrier discharge plasma. *Food Control, 47*, 451–456. https://doi.org/10.1016/j.foodcont.2014.07.053
Kopuk, B., Gunes, R., & Palabiyik, I. (2022). Cold plasma modification of food macromolecules and effects on related products. *Food Chemistry, 382*, Article 132356. https://doi.org/10.1016/j.foodchem.2022.132356
Korachi, M., Ozen, F., Aslan, N., Vannini, L., Guerzoni, M. E., Gottardi, D., & Ekinci, F. Y. (2015). Biochemical changes to milk following treatment by a novel, cold atmospheric plasma system. *International Dairy Journal, 42*, 64–69. https://doi.org/10.1016/j.idairyj.2014.10.006
Larkin, P. J. (2011). *Infrared and raman spectroscopy: Principles and spectral interpretation.* Elsevier.
Lassa, H., Jagielski, T., & Malinowski, E. (2011). Effect of different heat treatments and disinfectants on the survival of *Prototheca zopfii*. *Mycopathologia, 171*(3), 177–182. https://doi.org/10.1007/s11046-010-9365-7
Le Saux, G., Plawinski, L., Nlate, S., Ripoche, J., Buffeteau, T., & Durrieu, M. C. (2016). Beneficial effect of covalently grafted α-MSH on endothelial release of inflammatory mediators for applications in implantable devices. *PLoS One, 11*(3), Article e0150706. https://doi.org/10.1371/journal.pone.0150706
Liang, Y., Li, J., Xue, Y., Tan, T., Jiang, Z., He, Y., Shangguan, W., Yang, J., & Pan, Y. (2021). Benzene decomposition by non-thermal plasma: A detailed mechanism study by synchrotron radiation photoionization mass spectrometry and theoretical calculations. *Journal of Hazardous Materials, 420*, Article 126584. https://doi.org/10.1016/j.jhazmat.2021.126584
Liang, Y., Xue, Y., Fang, D., Tan, T., Jiang, Z., Shangguan, W., Yang, J., & Pan, Y. (2024). Reaction mechanism of toluene decomposition in non-thermal plasma: How does it compare with benzene? *Fundamental Research, 4*, 1100–1109. https://doi.org/10.1016/j.fmre.2022.03.026
Liao, X., Liu, D., Xiang, Q., Ahn, J., Chen, S., Ye, X., & Ding, T. (2017). Inactivation mechanisms of non-thermal plasma on microbes: A review. *Food Control, 75*, 83–91. https://doi.org/10.1016/j.foodcont.2016.12.021
Libisch, B., Picot, C., Ceballos-Garzon, A., Moravkova, M., Klimesová, M., Telkes, G., … Le Pape, P. (2022). *Prototheca* infections and ecology from a one health perspective. *Microorganisms, 10*, Article 938. https://doi.org/10.3390/microorganisms10050938
Liu, F., Lai, S., Tong, H., Lakey, P. S. J., Shiraiwa, M., Weller, M. G., … Kampf, C. J. (2017). Release of free amino acids upon oxidation of peptides and proteins by hydroxyl radicals. *Analytical and Bioanalytical Chemistry, 409*, 2411–2420. https://doi.org/10.1007/s00216-017-0188-y
Melville, P. A., Watanabe, E. T., Benites, N. R., Ribeiro, A. R., Silva, J. A. B., Garino, F., & Costa, E. O. (1999). Evaluation of the susceptibility of *Prototheca zopfii* to milk pasteurization. *Mycopathologia, 146*, 79–82. https://doi.org/10.1023/A:1007005729711
Moosavi, M. H., Khani, M. R., Shokri, B., Hosseini, S. M., Shojaee-Aliabadi, S., & Mirmoghtadaie, L. (2020). Modifications of protein-based films using cold plasma. *International Journal of Biological Macromolecules, 142*, 769–777. https://doi.org/10.1016/j.ijbiomac.2019.10.017
Moszczyńska, J., Roszek, K., & Wiśniewski, M. (2023). Non-thermal plasma application in medicine—Focus on reactive species involvement. *International Journal of Molecular Sciences, 24*, Article 12667. https://doi.org/10.3390/ijms241612667
Murtaza, B., Wang, L., Li, X., Saleemi, M. K., Nawaz, M. Y., Li, M., & Xu, Y. (2024). Cold plasma: A success road to mycotoxins mitigation and food value edition. *Food Chemistry*, *445*, article 138378. doi:https://doi.org/10.1016/j.foodchem.2024.138378.
Nakamoto, K. (2009). *Infrared and Raman spectra of inorganic and coordination compounds* (6th ed.). John Wiley & Sons. https://doi.org/10.1002/9780470405840 (Chapter 2).
Nardoni, S., & Mancianti, F. (2023). *Prototheca* spp. in bovine infections. *Encyclopedia, 3*, 1121–1132. https://doi.org/10.3390/encyclopedia3030081
Ng, S. W., Lu, P., Rulikowska, A., Boehm, D., O'Neill, G., & Bourke, P. (2021). The effect of atmospheric cold plasma treatment on the antigenic properties of bovine milk casein and whey proteins. *Food Chemistry, 342*, Article 128283. https://doi.org/10.1016/j.foodchem.2020.128283
Nguyen, T., Palmer, J., Phan, N., Shi, H., Keener, K., & Flint, S. (2022). Control of aflatoxin M1 in skim milk by high voltage atmospheric cold plasma. *Food Chemistry, 386*, Article 132814. https://doi.org/10.1016/j.foodchem.2022.132814
Nielsen, E. B., & Schellman, J. A. (1967). The absorption spectra of simple amides and peptides. *The Journal of Physical Chemistry, 71*(7), 2297–2304. https://doi.org/10.1021/j100866a051
Niessen, W. M. A., & Falck, D. (2015). Introduction to mass spectrometry, a tutorial. In J. Kool, & W. M. A. Niessen (Eds.), *Analyzing biomolecular interactions by mass spectrometry (chapter 1)*. Wiley-VCH.
Oehmigen, K., Hähnel, M., Brandenburg, R., Wilke, C., Weltmann, K. D., & Von Woedtke, T. (2010). The role of acidification for antimicrobial activity of atmospheric pressure plasma in liquids. *Plasma Processes and Polymers, 7*(3–4), 250–257. https://doi.org/10.1002/ppap.200900077
Otagiri, M., & Chuang, V. T. G. (2009). Pharmaceutically important pre- and posttranslational modifications on human serum albumin. *Biological and Pharmaceutical Bulletin, 32*(4), 527–534. https://doi.org/10.1248/bpb.32.527
Padmanaban, A., & Menon, S. (2017). *Characterization of mAb aggregation using a Cary 60 UV-Vis spectrophotometer and Agilent 1260 infinity LC system.* Agilent Technologies Publication, 5991-7974EN.
Pankaj, S. K., Wan, Z., & Keener, K. M. (2018). Effects of cold plasma on food quality: A review. *Foods, 7*, Article 4. https://doi.org/10.3390/foods7010004
Ponraj, S. B., Sharp, J. A., Kanwar, J. R., Sinclair, A. J., Kviz, L., Nicholas, K. R., & Dai, X. J. (2017). Argon gas plasma to decontaminate and extend shelf life of milk. *Plasma Processes and Polymers, 14*(11), Article 1600242. https://doi.org/10.1002/ppap.201600242
Poulsen, N. A., Eskildsen, C. E., Akkerman, M., Johansen, L. B., Hansen, M. S., Hansen, P. W., … Larsen, L. B. (2016). Predicting hydrolysis of whey protein by mid-infrared spectroscopy. *International Dairy Journal, 61*, 44–50. https://doi.org/10.1016/j.idairyj.2016.04.002
Ramirez-Alvarado, M., Kortemme, T., Blanco, F. J., & Serrano, L. (1999). β-Hairpin and β-sheet formation in designed linear peptides. *Bioorganic & Medicinal Chemistry, 7*(1), 93–103. https://doi.org/10.1016/S0968-0896(98)00215-6
Rao, K. S., Senthilnathan, J., Ting, J. M., & Yoshimura, M. (2014). Continuous production of nitrogen-functionalized graphene nanosheets for catalysis applications. *Nanoscale, 6*, 12758–12768. https://doi.org/10.1039/c4nr02824d
Rathod, N. B., Kahar, S. P., Ranveer, R. C., & Annapure, U. S. (2021). Cold plasma an emerging nonthermal technology for milk and milk products: A review. *International Journal of Dairy Technology, 74*(4), 615–626. https://doi.org/10.1111/1471-0307.12771
Raynal, B., Lenormand, P., Baron, B., Hoos, S., & England, P. (2014). Quality assessment and optimization of purified protein samples: Why and how? *Microbial Cell Factories, 13*, Article 180. https://doi.org/10.1186/s12934-014-0180-6
Reuter, S., Von Woedtke, T., & Weltmann, K. D. (2018). The kINPen—A review on physics and chemistry of the atmospheric pressure plasma jet and its applications. *Journal of Physics D: Applied Physics, 51*, Article 233001. https://doi.org/10.1088/1361-6463/aab3ad
Rivelli Zea, S. M., Itoh, M., & Toyotome, T. (2024). Development of loop-mediated isothermal amplification for the detection of *Prototheca bovis* directly from milk samples of dairy cattle. *Mycopathologia, 189*, Article 1. https://doi.org/10.1007/s11046-023-00806-1

Sarangapani, C., Danaher, M., Tiwari, B., Lu, P., Bourke, P., & Cullen, P. J. (2017). Efficacy and mechanistic insights into endocrine disruptor degradation using atmospheric air plasma. *Chemical Engineering Journal, 326*, 700–714. https://doi.org/10.1016/j.cej.2017.05.178

Sarangapani, C., Keogh, D. R., Dunne, J., Bourke, P., & Cullen, P. J. (2017). Characterisation of cold plasma treated beef and dairy lipids using spectroscopic and chromatographic methods. *Food Chemistry, 235*, 324–333. https://doi.org/10.1016/j.foodchem.2017.05.016

Satoh, A. Y., Trosko, J. E., & Masten, S. J. (2007). Methylene blue dye test for rapid qualitative detection of hydroxyl radicals formed in a Fenton's reaction aqueous solution. *Environmental Science and Technology, 41*(8), 2881–2887. https://doi.org/10.1021/es0617800

Segat, A., Misra, N. N., Cullen, P. J., & Innocente, N. (2015). Atmospheric pressure cold plasma (ACP) treatment of whey protein isolate model solution. *Innovative Food Science and Emerging Technologies, 29*, 247–254. https://doi.org/10.1016/j.ifset.2015.03.014

Segat, A., Misra, N. N., Cullen, P. J., & Innocente, N. (2016). Effect of atmospheric pressure cold plasma (ACP) on activity and structure of alkaline phosphatase. *Food and Bioproducts Processing, 98*, 181–188. https://doi.org/10.1016/j.fbp.2016.01.010

Seshadri, S., Khurana, R., & Fikn, A. L. (1999). Fourier transform infrared spectroscopy in analysis of protein deposits. *Methods in Enzymology, 309*, 559–576. https://doi.org/10.1016/S0076-6879(99)09038-2

Sharma, S., & Singh, R. K. (2022). Effect of atmospheric pressure cold plasma treatment time and composition of feed gas on properties of skim milk. *LWT - Food Science and Technology, 154*, Article 112747. https://doi.org/10.1016/j.lwt.2021.112747

Silva, W. M., Ribeiro, H., Seara, L. M., Calado, H. D. R., Ferlauto, A. S., Paniago, R. M., … Silva, G. G. (2012). Surface properties of oxidized and aminated multi-walled carbon nanotubes. *Journal of the Brazilian Chemical Society, 23*(6), 1078–1086. https://doi.org/10.1590/S0103-50532012000600012

Silverstein, R. M., Webster, F. X., & Kiemle, D. J. (2005). *Spectrometric identification of organic compounds* (7th ed.). John Wiley & Sons.

Siow, K. S., Britcher, L., Kumar, S., & Griesser, H. J. (2018). XPS study of sulfur and phosphorus compounds with different oxidation states. *Sains Malaysiana, 47*(8), 1913–1922. https://doi.org/10.17576/jsm-2018-4708-33

Stuart, B. H. (2004). *Infrared spectroscopy: Fundamentals and applications*. John Wiley & Sons. https://doi.org/10.1002/0470011149.fmatter

Su, J. Y., Hodges, R. S., & Kay, C. M. (1994). Effect of chain length on the formation and stability of synthetic α-helical coiled coils. *Biochemistry, 33*(51), 15501–15510. https://doi.org/10.1021/bi00255a032

Surowsky, B., Schlüter, O., & Knorr, D. (2015). Interactions of non-thermal atmospheric pressure plasma with solid and liquid food systems: A review. *Food Engineering Reviews, 7*(2), 82–108. https://doi.org/10.1007/s12393-014-9088-5

Swift, P. (1982). Adventitious carbon—The panacea for energy referencing? *Surface and Interface Analysis, 4*(2), 47–51. https://doi.org/10.1002/sia.740040204

Szczerska, M., Kosowska, M., Gierowski, J., Cieślik, M., Sawczak, M., & Jakóbczyk, P. (2023). Investigation of the few-layer black phosphorus degradation by the photonic measurements. *Advanced Materials Interfaces, 10*, Article 2202289. https://doi.org/10.1002/admi.202202289

Szyk-Warszyńska, L., Raszka, K., & Warszyński, P. (2019). Interactions of casein and polypeptides in multilayer films studied by FTIR and molecular dynamics. *Polymers, 11*, Article 920. https://doi.org/10.3390/polym11050920

Takai, E., Kitamura, T., Kuwabara, J., Ikawa, S., Yoshizawa, S., Shiraki, K., Kawasaki, H., Arakawa, R., & Kitano, K. (2014). Chemical modification of amino acids by atmospheric-pressure cold plasma in aqueous solution. *Journal of Physics D: Applied Physics, 47*, Article 285403. https://doi.org/10.1088/0022-3727/47/28/285403

Tange, K., Nomura, S., & Nakajina, J. (2020). Methylene blue decomposition via various in-liquid plasma methods. *Journal of the Japan Institute of Energy, 99*(8), 93–103. https://doi.org/10.3775/jie.99.99

Trivedi, M. K., Branton, A., Trivedi, D., Nayak, G., Mishra, R. K., & Jana, S. (2015). Physicochemical evaluation of biofield treated peptone and Malmgren modified terrestrial orchid medium. *American Journal of Bioscience and Bioengineering, 3*(6), 169–177. https://doi.org/10.11648/j.bio.20150306.15

Trivedi, M. K., Nayak, G., Patil, S., Tallapragada, R. M., Jana, S., & Mishra, R. (2015). Evaluation of the impact of biofield treatment on physical and thermal properties of casein enzyme hydrolysate and casein yeast peptone. *Clinical Pharmacology & Biopharmaceutics, 4*(2), Article 1000138. https://doi.org/10.4172/2167-065x.1000138

Tyczkowska-Sieroń, E., Kapica, R., Markiewicz, J., & Tyczkowski, J. (2018). Linear microdischarge jet for microbiological applications. *Plasma Medicine, 8*(1), 57–71. https://doi.org/10.1615/PlasmaMed.2018024459

Tyczkowska-Sieroń, E., Markiewicz, J., Grzesiak, B., Krukowski, H., Głowacka, A., & Tyczkowski, J. (2018). Cold atmospheric plasma inactivation of *Prototheca zopfii* isolated from bovine milk. *Journal of Dairy Science, 101*(1), 118–122. https://doi.org/10.3168/jds.2017-13262

Varodi, C., Pogăcean, F., Cioriță, A., Pană, O., Leoștean, C., Cozar, B., … Pruneanu, S. M. (2021). Nitrogen and sulfur co-doped graphene as efficient electrode material for l-cysteine detection. *Chemosensors, 9*, Article 146. https://doi.org/10.3390/chemosensors9060146

Verlackt, C. C. W., Van Boxem, W., Dewaele, D., Lemière, F., Sobott, F., Benedikt, J., … Bogaerts, A. (2017). Mechanisms of peptide oxidation by hydroxyl radicals: Insight at the molecular scale. *Journal of Physical Chemistry C, 121*(10), 5787–5799. https://doi.org/10.1021/acs.jpcc.6b12278

Wang, S., Liu, Y., Zhang, Y., Lü, X., Zhao, L., Song, Y., Zhang, L., Jiang, H., Zhang, J., & Ge, W. (2022). Processing sheep milk by cold plasma technology: Impacts on the microbial inactivation, physicochemical characteristics, and protein structure. *LWT - Food Science and Technology, 153*, Article 1125573. https://doi.org/10.1016/j.lwt.2021.112573

Wenske, S., Lackmann, J. W., Busch, L. M., Bekeschus, S., von Woedtke, T., & Wende, K. (2021). Reactive species driven oxidative modifications of peptides—Tracing physical plasma liquid chemistry. *Journal of Applied Physics, 129*, Article 193305. https://doi.org/10.1063/5.0046685

Whitehead, K. A., Benson, P. S., & Verran, J. (2011). The detection of food soils on stainless steel using energy dispersive X-ray and Fourier transform infrared spectroscopy. *Biofouling, 27*(8), 907–917. https://doi.org/10.1080/08927014.2011.611879

Xu, G., & Chance, M. R. (2007). Hydroxyl radical-mediated modification of proteins as probes for structural proteomics. *Chemical Reviews, 107*(8), 3514–3543. https://doi.org/10.1021/cr0682047

Yao, L., Zhou, Z., Wang, S., Zou, Q., Wang, H. X., Ma, L. X., … Zhang, X. (2022). Phosphorylation of covalent organic framework nanospheres for inhibition of amyloid-β peptide fibrillation. *Chemical Science, 13*(20), 5902–5912. https://doi.org/10.1039/d2sc00253a

Zhang, J., Song, J., Wang, S., Su, Y., Wang, L., & Ge, W. (2024). The casein in sheep milk processed by cold plasma technology: Phosphorylation degree, functional properties, oxidation characteristics, and structure. *Food Chemistry, 457*, Article 1401400. https://doi.org/10.1016/j.foodchem.2024.140140

Zhang, Q., Ma, R., Tian, Y., Su, B., Wang, K., Yu, S., Zhang, J., & Fang, J. (2016). Sterilization efficiency of a novel electrochemical disinfectant against *Staphylococcus aureus*. *Environmental Science and Technology, 50*(6), 3184–3192. https://doi.org/10.1021/acs.est.5b05108

Zhou, R., Zhou, R., Wang, P., Xian, Y., Mai-Prochnow, A., Lu, X., … Bazaka, K. (2020). Plasma-activated water: Generation, origin of reactive species and biological applications. *Journal of Physics D: Applied Physics, 53*(30), Article 303001. https://doi.org/10.1088/1361-6463/ab81cf

Zhou, R., Zhou, R., Zhuang, J., Zong, Z., Zhang, X., Liu, D., … Ostrikov, K. (2016). Interaction of atmospheric-pressure air microplasmas with amino acids as fundamental processes in aqueous solution. *PLoS One, 11*(5), Article e0155584. https://doi.org/10.1371/journal.pone.0155584